MASTER'S THESIS

DIVISION OF MATERIALS ENGINEERING

June 2017

CHARACTERISATION OF PACKAGING MATERIAL SURFACES

Authors: Mikael Ek & Andreas Ingelström

Supervisors: Professor Dmytro Orlov, LUND UNIVERSITY
Dr. Martin Adell, Tetra Pak Packaging Solutions AB

Examiner: Professor Srinivasan Iyengar, LUND UNIVERSITY

LUND UNIVERSITY

MSc Thesis
ISRN LUTFD2/TFMT--17/5054--SE

Department of Mechanical Engineering
Lund University
Box 118
SE-221 00 LUND
Sweden

©Mikael Ek & Andreas Ingelström. All rights reserved.
Printed in Sweden
Lund 2017

Abstract

As the packaging material (PM) becomes better defined from the results of technical development, its processing stages will be of greater complexity. The nip process is an example of one vital step in the lamination coating of PM, and this process is studied in the present thesis by analysing the surfaces of chill rollers (CR) and PM. Ideally, a laminated PM surface should be the perfect negative of a CR surface, and a correlation between the features of these surfaces is of significant importance. More specifically, a set of surface texture parameters was used to compare the corresponding surfaces and to reveal the dependence of PM properties on its surface texture. To determine the surface texture parameters, a focus variation microscope was used to study both CR and PM surfaces. The gloss of PM was studied by ocular observation for both inside and décor sides. These results were compared to the surface parameters for finding characteristics that can offer the explanation of difference in gloss. Such an explanation was found in the differences between CR and PM surface textures. The friction of PM against metal surface was studied for three PM samples, including both inside and décor sides. While no direct correlation between surface parameters and friction data could be found, a hypothesis explaining the differences is presented.

Keywords: packaging material, surface texture, focus variation, 3D measurement, pattern transfer, glossiness, friction

This thesis is dedicated to the vuvuzela that was never mentioned.

Acknowledgements

First, we would like to thank our main supervisor Professor Dmytro Orlov of the Materials Engineering department at Lund University along with company supervisor Dr. Martin Adell who is Technology Specialist at Tetra Pak Packaging Solutions AB in Lund for their extensive aid and merit in the field during this project. Without their passionate participation and input, this thesis could not have been successfully completed.

Second, we would like to thank Karin Strömberg, Manager Nip Technology at Tetra Pak Packaging Solutions AB, for checking the report and her support with administrative issues related to this project.

We would also like to thank Annika Lindbäck, a Laboratory Technician at Tetra Pak Packaging Solutions AB. Her help in performing friction measurements enabled us to include a valuable part to the project.

Sincere grateful thanks also go to our examiner Professor Srinivasan Iyengar of the Materials Engineering department at Lund University for reading and checking the project report.

Finally, we express very deep gratitude to our families for providing us with unfailing support and continuous encouragement throughout our years of study and through the process of researching and writing this thesis. This accomplishment would not have been possible without them. Thank you.

Mikael Ek & Andreas Ingelström

Sammanfattning på svenska

I lamineringsprocessen på Tetra Pak ingår tre steg, eller tre *nyp*, där ytan av den färdiga produkten definieras. I nypet trycks en polymersmälta och ett blivande förpackningsmaterial (*packaging material*, PM) ihop av en nypvals mot en kylvals (*chill roller*, CR). I den bästa av världar får man ett direkt negativ av CR-ytan på polymerfilmen. Då flera faktorer influerar överföringen av ytstrukturen ser verkligheten inte ut så. Hur bra negativ man får är idag inte tillräckligt studerat och det kräver djupare analys för att förstå och bättre kunna optimera CR-ytan.

Insidan och utsidan, även kallad dekorsidan, av PM:et kräver olika egenskaper. På insidan spelar funktionella egenskaper som friktion en viktig roll och på dekorsidan är utseendet av större betydelse. Dessa egenskaper karakteriseras av ytstrukturer och genom att mappa dessa mot varandra vill man skapa en grundligare förståelse av hur CR-ytan påverkar PM:ets egenskaper.

Med andra ord, målet är att dessa två delar ska börja förklara kopplingen mellan CR-yta och egenskaper hos färdigt PM som man ser på hyllor i dagligvaruhandeln.

Division of report

When writing this report, both authors contributed equally. In these statements, we indicate who of the authors wrote the majority of respective (sub)sections.

Mikael Ek wrote:

- Abstract
- Review of surface metrology
  - 3D surface parameters
  - Gloss
  - Friction
- Results and Discussion
  - Décor PM surfaces
  - Properties of PM
- Future work

Andreas Ingelström wrote:

- Review of surface metrology
  - Introduction
  - Topography and its metrology
- Objectives
- Experiments
- Results and Discussion
  - Inside PM surfaces
  - Outlier analysis
- Conclusions

Contents

Nomenclature

mr	Material ratio
$\mathbf{S_a}$	Average roughness
$\mathbf{S_k}$	Core roughness depth
$\mathbf{S_p}$	Maximum peak height
$\mathbf{S_q}$	Root mean square roughness
$\mathbf{S_v}$	Maximum valley depth
$\mathbf{S_z}$	Maximum height
$\mathbf{S_{10z}}$	Ten-point height average
$\mathbf{S_{dq}}$	Root mean square surface slope
$\mathbf{S_{dr}}$	Development interfacial area ratio
$\mathbf{S_{ku}}$	Kurtosis
$\mathbf{S_{mr1}}$	Peak material portion
$\mathbf{S_{mr2}}$	Valley material portion
$\mathbf{S_{pk}}$	Reduced peak height
$\mathbf{S_{sk}}$	Skewness
$\mathbf{S_{vk}}$	Reduced valley depth
$\mathbf{V_v}$	Void volume
$\mathbf{V_{mc}}$	Core material volume
$\mathbf{V_{mp}}$	Peak material volume
$\mathbf{V_{vc}}$	Core void volume
$\mathbf{V_{vv}}$	Dale void volume
CoF	Coefficient of friction
CR	Chill roller
PM	Packaging material

List of Figures

1 Review of surface metrology

The surfaces of Tetra Pak packaging material (PM) have big impact on several different aspects including final products seen on shelves in stores, converting process and filling machines. One area where such surfaces play a major role is optical appearance, *i.e.* how the printed décor is perceived. Another area is mechanical properties such as friction that is also determined by PM surface texture to a large extent. Friction is a very important parameter in the production of PM as well as forming, filling and the performance of final package. Good understanding and control of surfaces of PM polymer and their properties are necessary as these surfaces have such a big impact on the production process, performance and the quality of package.

PM surfaces are formed, and thus given their structure, in nips during the process of lamination. A schematic image displaying main parts in the nip is shown in Figure 1.1. The lamination process at Tetra Pak has three nips, and in each of these a molten polymer film is solidified onto the packaging material structure. In Figure 1.2, a schematic cross-section of the PM structure showing the layers that form it can be seen. The texture of metal chill roller (CR) surfaces plays a dominant role when creating the surface of PM. Other process parameters also influence the structures of final surface. Namely, PM surfaces will not be simply the negative of CR surfaces, but will vary due to different process variables. Therefore, to create a specific surface, both the effects of CR surfaces and process variables need to be mapped and understood. In addition, understanding of how different PM surface textures influence visual and mechanical properties of the polymer layers needs to be elaborated in order to optimize production processes and achieve the desired quality and appearance of Tetra Pak products.

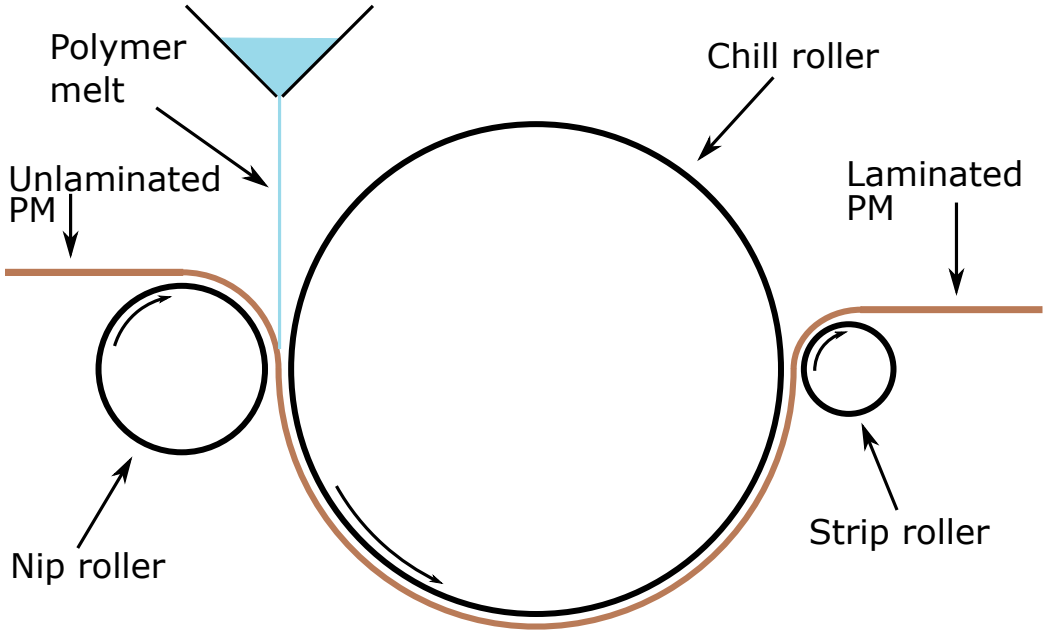

Figure 1.1 – Schematic view of the nip, where polymer melt is pressed onto PM. The nip takes place when the nip roller is pressed to the chill roller.

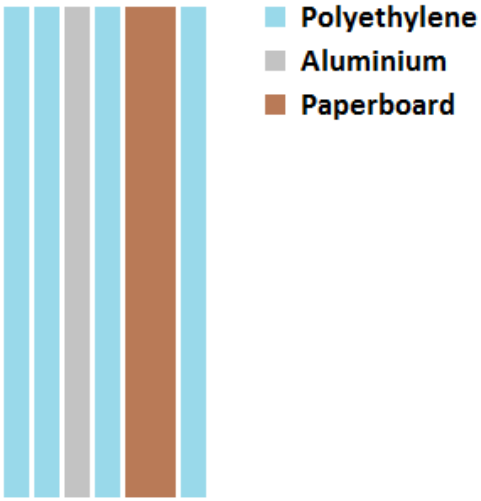

Figure 1.2 – Schematic view of a PM cross-section, indicating the position of polymer layers. The leftmost polyethylene layer represents the inside layer and the rightmost represents the décor layer.

1.1 Introduction

The history of paper in packaging industry goes back centuries before Tetra Pak came into the picture. In this section, the marriage of the two is explained. After that, a brief presentation of how surface characterisation has been performed and used over the years is introduced.

1.1.1 Paper packaging and Tetra Pak

Paper has been a component of interest when designing PM for a long time. In the middle of the seventeenth century, a patent called 'The way and art of making blew paper used by sugar-bakers and others' was granted to Hildeyerd, and this is recognized as one of the first references to using paper for packaging purposes. The use of paper accelerated during the nineteenth century as the manufacturing industry entered the industrial era. Today, over 40% of the entire paper and paperboard consumption in Europe is used for packaging with over 50% entitled to food packaging.[1]

Tetra Pak's entry into the packaging industry originates from the idea of Ruben Rausing in the early 1940s. The idea was to develop a package that required minimum amount of material, but at the same time maintained maximum hygienic standards. The idea became a reality in 1944 when the invention of tetrahedron-shaped carton package came, and eight years later the first machine producing the packages was delivered to a local dairy company. The foundation of Tetra Pak became a fact.[2]

Tetra Pak has been in a frontline position in the industry ever since. Therefore, it faces new challenges in the pursuit to create modern state-of-the-art packaging products. In this thesis, one of such challenges is addressed.

1.1.2 Historical development of surface characteristics assessment

Before any instrument for analysing surface topography was invented, observers simply used their fingernails to run across the surface of an object in order to get an idea of how rough or smooth it was. Even today, the fundamental principles of such tactile comparison techniques are used when the surface of an object is compared manually to a set of calibrated surfaces of different known roughnesses.

To understand surfaces more accurately and to quantify their characteristics, a profilometer, or perthometer, was invented in the early twentieth century. An image illustrating the fundamental principles of a profilometer is shown in Figure 1.3. This surface assessment technique enables an observer to measure and to record deviations on a selected line on a surface. The technique consists of a stylus instrument that is moved along a line of

a surface to measure vertical deviations. The movement of stylus is subsequently recorded onto a photosensitive paper. In this way, peaks and valleys on the surface can be characterised by defining a simple set of parameters such as the average of five highest peaks or lowest valleys.

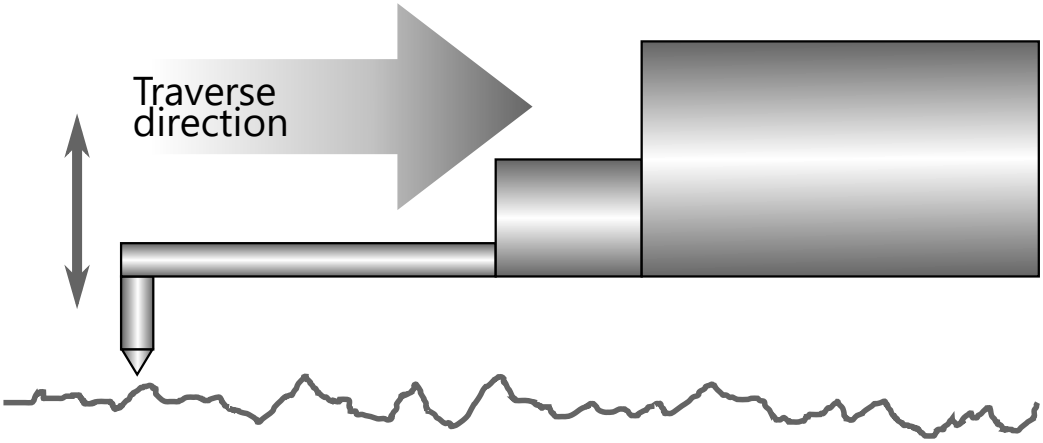

Figure 1.3 – The principles of a profilometer. Reproduced from Figure 2 in [3].

The mechanical function of profilometer was converted into an electronic counterpart as the technology advanced. Shortly after the profilometer was accepted, an electronic surface profile was created using analogue electronics. This made a way for new parameters describing surfaces, which enabled surface roughness to be averaged for the first time. One parameter in particular was named centre line average roughness (CLA), and then reduced to average roughness ($\mathbf{R_a}$). As the technology spread into laboratories all over the world, new parameters evolved, such as root mean square of surface roughness ($\mathbf{R_q}$) or peak height and valley depth ($\mathbf{R_t}$ and $\mathbf{R_z}$). Various sets of parameters were preferred by different scientist groups, and it took some time for a global standard to be introduced.[4] In the late twentieth century, the ISO standards 1302, 4287 and 13565 were published in order to globally standardise the use of surface texture parameters using a 2D profile method.[5]

In parallel with the introduction of these ISO standards, a group at the University of Birmingham began investigations under the lead of Stout that became the foundation of 3D surface texture standards of today. The group saw a need to develop improved standards different from those used in 2D profilometry and thus enabling the characterisation of surface textures from the analyses by new 3D measurement techniques. These efforts resulted in a famous publication *Blue book* ordered by the European Commission in

which fourteen 3D parameters were introduced; the "Birmingham 14 parameters".[6] A following program lead by Blunt made further research in the stability of the initial parameters, and studied their relevance to the functional criteria used by industries. This work lead to the creation of the ISO 25178 standard in 2005.[4]

Several techniques have been invented to analyse 3D surface parameters of various objects using the parameters in ISO 25178 as a base. This can be a raster scanning with a stylus instrument or more modern non-contact instruments based on *e.g.* confocal chromatic probing, coherence scanning interferometry or focus variation, as is the case with an instrument used at Tetra Pak. All types of techniques received a specific document of standard branched from the original ISO 25178. In the case of instruments based on focus variation, the document used is part 606 (nominal characteristics of non-contact (focus variation) instruments (ISO 25178-606:2015)).[7]

1.2 Topography and its metrology

'Topography' originates from Greek meaning "place" (topos) and "writing" (graphia), and it is often mentioned as surface texture in this report. It is characterised through components such as lay, roughness and waviness of a surface. The components are displayed in Figure 1.4. Lay is defined as the direction of predominant surface pattern. Roughness is mainly short wavelength features in a surface pattern. Its height is measured as the distance from a reference plane on the surface determined by operator in combination with a mathematical fitting. Roughness width is the distance between peaks or valleys that forms the lay of a surface. To obtain these variables, a roughness cut-off width is defined in a measurement, and needs to be greater than the roughness width of the lay. Parameters used to quantify surface roughness are all presented in Section 1.3, and are defined in ISO 25178. Waviness is the description of longer wavelength features on the surface that is outside of the roughness cut-off width. Similarly to roughness, it can be characterised by its height and width.[8]

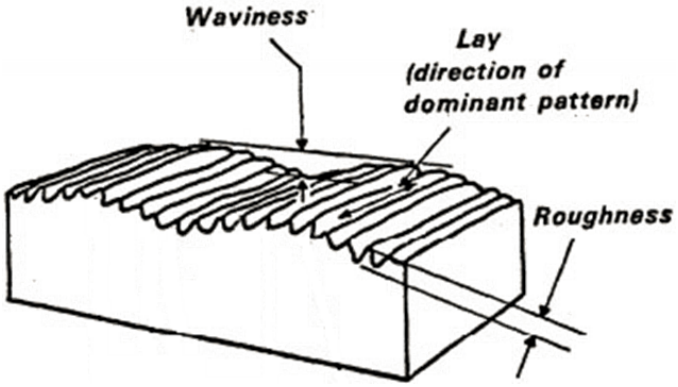

Figure 1.4 – The three general components describing surface texture. Modified from figure in [9].

The metrology behind topography is a complex field involving a large range of parameters. For a long time dominated by contact instrumentation (profilometers) displaying 2D (profile) information, the field today consist of many non-contact methods to analyse the 3D nature of an object's surface.[10] Non-contact 3D microscopes bring many advantages to the analysis of a surface compared to a profile counterpart. The profile analysis will work at its best for a known stable operating surface since it only gives a discrete vector of data. In contrast, 3D analysis will give data from an area, enabling users to *e.g.* identify a specific contour line as a part of a valley or a saddle point. Though, 3D analysis handles more complex and bigger sets of data and thus requires more time to perform an analysis.[11] A non-contact characterisation method using focus variation is described in the next section.

1.2.1 Focus variation instrument

A focus variation instrument can create a 3D image of an object's surface by sensing the variation of focus while vertically scanning the surface using optics with limited focus depth. In Figure 1.5, the schematics of using such an instrument is shown. White light is transmitted from an LED light source through a beam splitting mirror into the optical axis. The light is carried towards the sample surface through the objective. Due to a varying landscape at the surface, the light will be reflected in different directions. Some amount of reflected light will go back through the instrument objective and illuminate a CCD sensor on the other side of the beam splitting mirror. By changing the vertical position of the objective in relation to the sample, the degree of focus will vary, and this change of focus is related to a shift in contrast at the CCD sensor. By continuously scanning the sample for all positions

on the sensor, a 3D image with topographical and colour information can be created. Only a small region of the surface can be analysed at a certain distance due to the small depth of field of the objective, which means that each region of the object is sharply focused.[12]

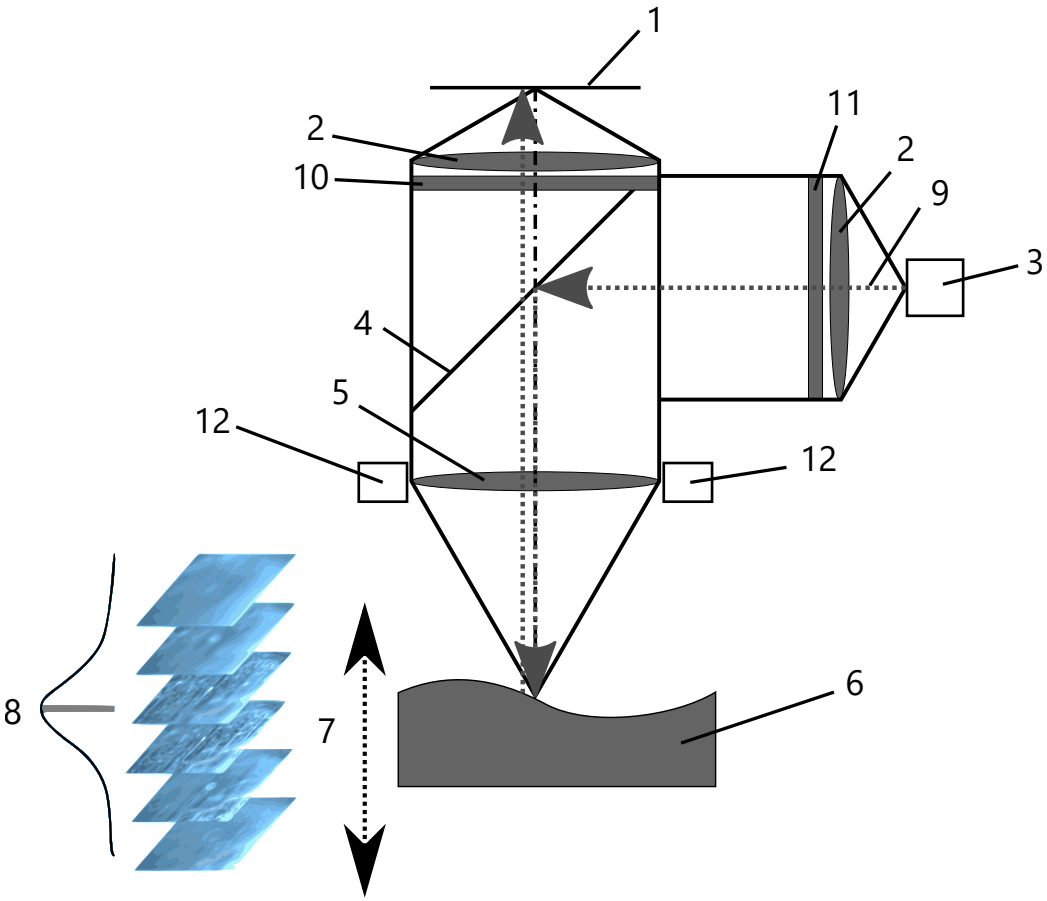

Figure 1.5 – The principles of focus variation technique. The numbers indicate: 1. Array detector, 2. Lenses, 3. White light source, 4. Beam splitter, 5. Objective, 6. Specimen, 7. Vertical scan, 8. Focus curve, 9. Light beam, 10. Analyser, 11. Polariser, 12. Ring light. Reproduced from Figure 1 in [12].

There are multiple ways to measure a shift in contrast, and hence focus variation, in an image of the CCD sensor. One method is to determine the standard deviation of pixel values in a local region bigger than the actual pixel size on the CCD sensor. This approach employs Equation 1.1.

$$F_z(x, y) = FM(reg_w(I_z, x, y)) \tag{1.1}$$

In Equation 1.1, the local region operator $reg_w(I_z, x, y)$ extracts information from the stacking of images I_z at a height z and at a lateral position (x, y) over a specific rectangular region of $w \times w$ pixels. This information is used to calculate the focus F_z with a focus measure FM.

Depending on how far from the CCD sensor the sample is located, hence how focused it will be, different standard deviations will be calculated. A pixel region out of focus will give similar pixel values and therefore a low variance and low standard deviation. Similarly, a region in focus will give a high standard deviation.

When the focus has been calculated for different z-positions, a focus curve can be drawn as can be seen in Figure 1.6.

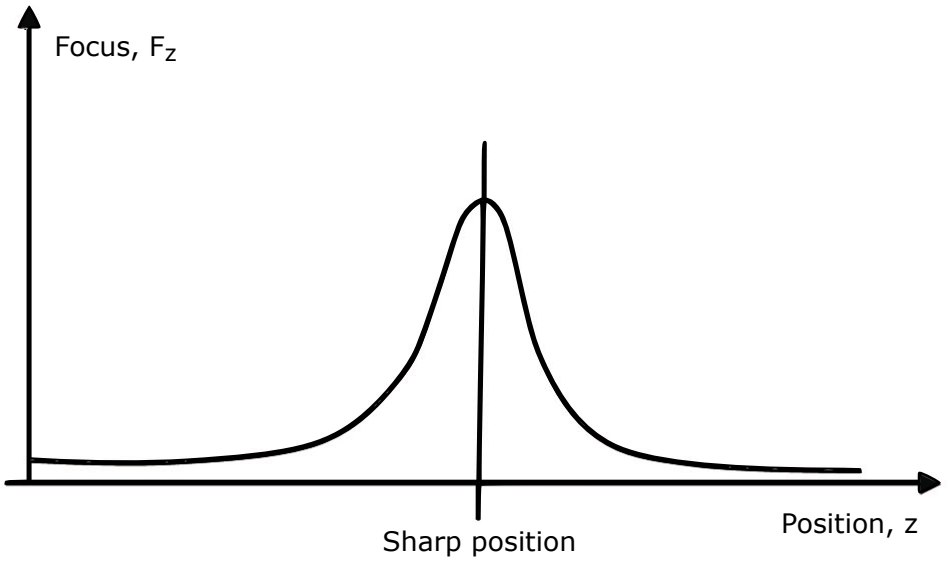

Figure 1.6 – Focus variation curve, where the focus is varied for different z-positions. The maximum point indicates the position where a pixel is in the best focus.

There are different ways to locate where the peak is. One is to simply determine the maximum value of the focus curve with n z axis positions, as is done in Equation 1.2.

$$\text{depth} = \arg(\max F_z) \text{ for } z_1 \leq z \leq z_n \tag{1.2}$$

When the maximum has been calculated for all lateral positions of the CCD detector, a depth map is received, and this is the tool used to construct 3D measurement results.[13]

1.3 3D surface parameters

The description of a surface topography requires a set of parameters. Such parameters can be divided into four categories: height parameters, spatial parameters, hybrid parameters and functional parameters. The spatial parameters are not described here since they have not been used in this study. All the parameters can be found with mathematical descriptions in the ISO 25178 standard.[7]

1.3.1 Height parameters

$\mathbf{S_a}$ and $\mathbf{S_q}$ are related to the average and the dispersion of the roughness distribution of a surface, and are called Average Roughness and Root Mean Square Roughness, respectively. These parameters represent the extent of surface deviation from a reference plane, and they are strongly correlated to each other.[4] The root mean square has more statistical significance (it is the standard deviation) and often has a more physical grounding than $\mathbf{S_a}$, *e.g.*, $\mathbf{S_q}$ is directly related to surface energy and the way light is scattered from a surface.

$\mathbf{S_p}$, $\mathbf{S_v}$ and $\mathbf{S_z}$ are parameters derived from the highest and the lowest points on a surface. $\mathbf{S_p}$ is the height of the highest peak and always positive, $\mathbf{S_v}$ is the depth of the lowest valley and $\mathbf{S_z}$ is the maximum height of the surface found from $\mathbf{S_z} = \mathbf{S_p} + |\mathbf{S_v}|$. $\mathbf{S_{10z}}$ is found from the average of five highest peaks and five deepest valleys, and can be assumed to be a more robust parameter than $\mathbf{S_p}$, $\mathbf{S_v}$ and $\mathbf{S_z}$.

$\mathbf{S_{sk}}$ is the Skewness of surface texture. It is a unit-less parameter since it is normalised by $\mathbf{S_q}$. $\mathbf{S_{sk}}$ can be used to describe the shape of the texture height distribution. More specifically, it represents the degree of symmetry about the mean plane of the surface. The sign of $\mathbf{S_{sk}}$ indicates a predominance of peaks $\mathbf{S_{sk} > 0}$ or valleys $\mathbf{S_{sk} < 0}$. For example, the value is zero for a surface that has symmetrical texture with a random (or Gaussian) height distribution. A surface with a positive skewness will presumably have poor lubricant retention because of the lack of deep valleys to retain lubricant traces in its texture. It correlates well with load carrying abilities and porosity of the studied sample, but it is strongly influenced by isolated peaks or valleys.

$\mathbf{S_{ku}}$ is the Kurtosis and it is a measure of sharpness of the surface height distribution. It is also normalised by $\mathbf{S_q}$, and hence it is a unit-less parameter. As a strictly positive parameter, it indicates the presence of excessively high peaks or deep valleys ($\mathbf{S_{ku} > 3}$) or lack thereof ($\mathbf{S_{ku} < 3}$).

$\mathbf{S_{sk}}$ and $\mathbf{S_{ku}}$ parameters use high order powers in their equations ($\mathbf{S_{sk}}$

three and $\mathbf{S_{ku}}$ four), which may lead to a lesser mathematical stability compared to other parameters, and thus leading to a faster error propagation.[14]

1.3.2 Hybrid parameters

As suggested by name, hybrid parameters are the mix of height and spatial parameters.

Root Mean Square Surface Slope, $\mathbf{S_{dq}}$, is the general measure of slopes comprising the surface. It can be used to differentiate surfaces with similar $\mathbf{S_q}$. It can be a unit-less parameter that adopts only positive values or presented as angles with a slight modification to its original definition. The parameter may be used to control the cosmetic appearance of a surface.

Development Interfacial Area Ratio, $\mathbf{S_{dr}}$, is expressed as the percentage of additional area contributed by texture, as compared to an ideal plane of the size of a measured region. It is usually given as a value of percentage, commonly between 0% and 10%, where 0% represents a perfectly flat surface. The parameter may be used to provide helpful correlations in adhesion applications.[14]

1.3.3 Functional parameters

Functional parameters are parameters that may give a direct indication to the functional properties of a surface.

Material Ratio, **mr**, is the ratio of the intersecting area of a plane (*i.e.* parallel to the reference plane) passing through the surface at a given height to the cross-sectional area of evaluation region. Areal Material Ratio Curve (*aka* Bearing Area Curve or Abbot-Firestone Curve) is established by evaluating **mr** at various levels from the highest peak to the lowest valley.

$\mathbf{S_{pk}}$, $\mathbf{S_k}$, $\mathbf{S_{vk}}$, $\mathbf{S_{mr1}}$ and $\mathbf{S_{mr2}}$ are all derived from the areal material ratio curve. They are shown in Figure 1.7. $\mathbf{S_{pk}}$ is Reduced Peak Height that is measured as the peak height above the core roughness. $\mathbf{S_k}$ is Core Roughness Depth that measures the core roughness of a surface with most extreme peaks and valleys removed. $\mathbf{S_{vk}}$ is Reduced Valley Depth, which measures valley depth below the core roughness. The two **mr** parameters, $\mathbf{S_{mr1}}$ and $\mathbf{S_{mr2}}$ are Peak Material Portion and Valley Material Portion, respectively. $\mathbf{S_{mr1}}$ indicates what percentage of material that forms the structures correlated with $\mathbf{S_{pk}}$. Correspondingly, $\mathbf{S_{mr2}}$ expresses what percentage of material that forms the valleys correlated with $\mathbf{S_{vk}}$.[15]

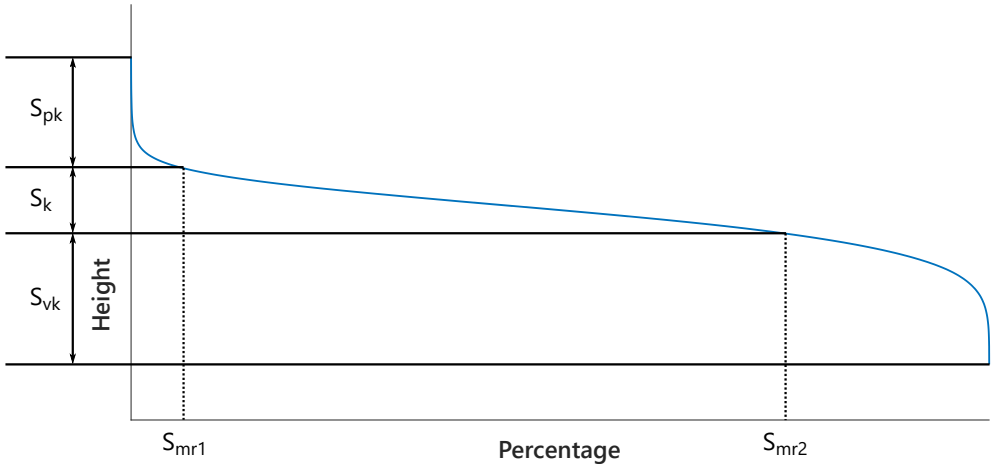

Figure 1.7 – Areal material ratio curve, indicating five functional parameters $\mathbf{S_{pk}}$, $\mathbf{S_k}$, $\mathbf{S_{vk}}$, $\mathbf{S_{mr1}}$ and $\mathbf{S_{mr2}}$.

$\mathbf{V_v(mr)}$, $\mathbf{V_{vv}(q)}$, and $\mathbf{V_{vc}(p,q)}$ relate to void volumes bound by the surface texture, and the latter two are shown in Figure 1.8. $\mathbf{V_v(mr)}$ is Void Volume bound by the surface texture from a plane at a height corresponding to a chosen **mr**-value to the lowest height of the surface. $\mathbf{V_{vv}(q)}$ is Dale Void Volume and it is similar to $\mathbf{V_v(mr)}$, but the height is determined by **mr**-value **q**, where **q** is 80% by default. $\mathbf{V_{vc}(p,q)}$ is Core Void Volume, a measure of volume bound by the surface texture at heights corresponding to the **mr**-values **p** and **q**, where **p** is 10% and **q** is 80% by default.[15]

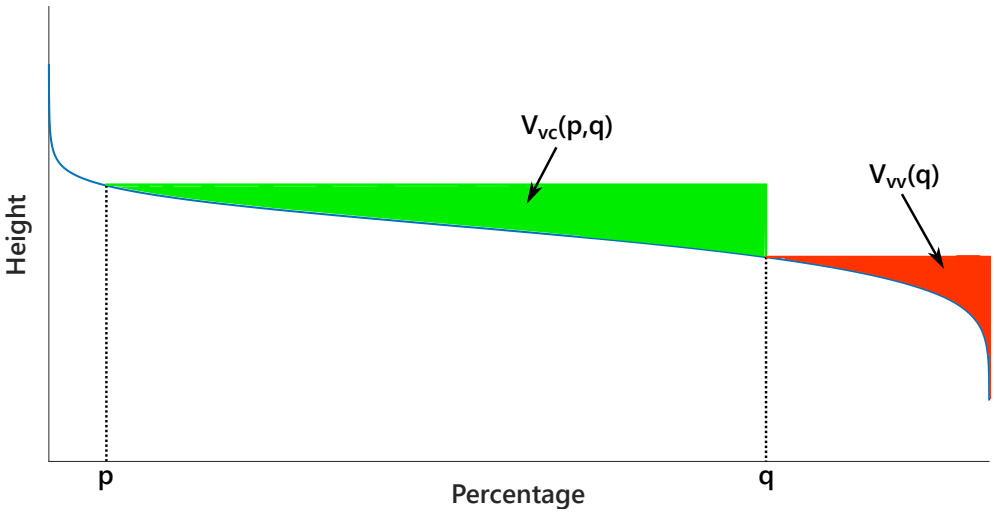

Figure 1.8 – Areal material ratio curve indicating functional parameters $\mathbf{V_{vc}}$ and $\mathbf{V_{vv}}$.

Similarly to void volumes, $\mathbf{V_{mp}}(\mathbf{p})$ and $\mathbf{V_{mc}}(\mathbf{p}, \mathbf{q})$ are parameters that define material volumes in the surface texture. They are shown in Figure 1.9. $\mathbf{V_{mp}}(\mathbf{p})$ is Peak Material Volume, a measure of the material that comprises the surface from a height corresponding to **mr**-value **p**. It may be used to characterise the volume of material that is likely to be removed during running-in of a component. $\mathbf{V_{mc}}(\mathbf{p}, \mathbf{q})$ is Core Material Volume, which is similar to $\mathbf{V_{mp}}$, but the range of material is limited by heights corresponding to two **mr**-values **p** and **q**.[15] This parameter is a measure of how much surface material that does not interact with another surface in contact, and which does not play any role in lubrication.[14]

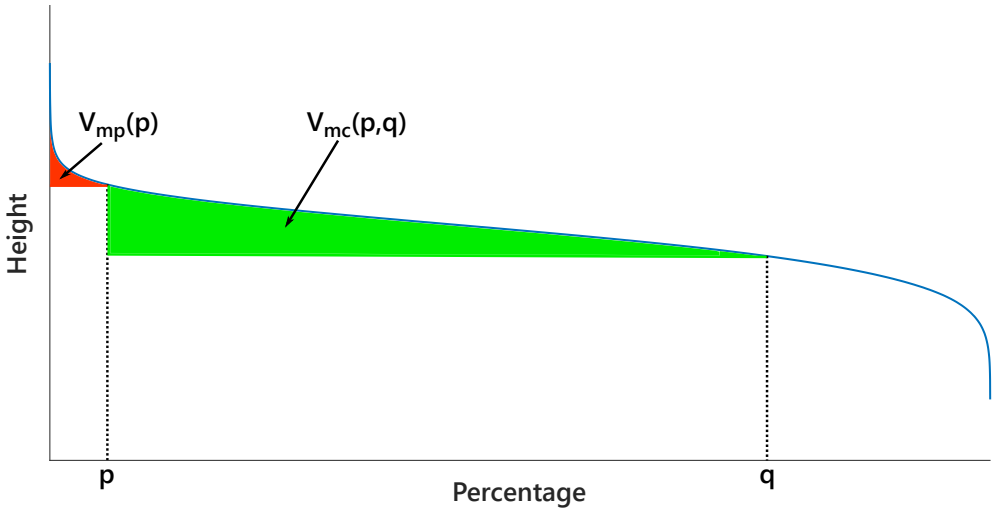

Figure 1.9 – Areal material ratio curve indicating two more functional parameters $\mathbf{V_{mp}}$ and $\mathbf{V_{mc}}$.

1.4 Gloss

Visual appearance is an important factor when producing packaging products since it affects the first impression of a customer, which is a great deal for a final consumer. As an important property to evaluate visual characteristics, the gloss is not to be ignored. It largely depends on how surface reflects incoming light. The property itself can be divided into several indicators where specular gloss is the most common one to study. Specular gloss corresponds to how bright specularly reflected light is perceived. Another indicator is haze, which is an indication of how cloudy a surface appear.[16] The gloss of a surface can be measured accurately by a glossometer, but in this thesis a more rough approach is employed where images of illuminated surfaces are taken. It should be noted that this approach is not standardised

in any way, but it gives the indication of gloss when comparing images.

1.5 Friction

Friction is a complex phenomenon. It is not the property of a specific material, but the property of a system. In the system, the objects experience two types of friction, *static* and *dynamic*. If one object is pulled on top of a surface, but not enough to get it moving, the object experiences static friction. Increasing the force which the object is pulled with, the friction increases until the threshold of motion. At the threshold, the object will start to move and now experience dynamic friction, which is lower than the static one. A schematic showing the Coefficient of Friction (CoF) is presented in Figure 1.10.

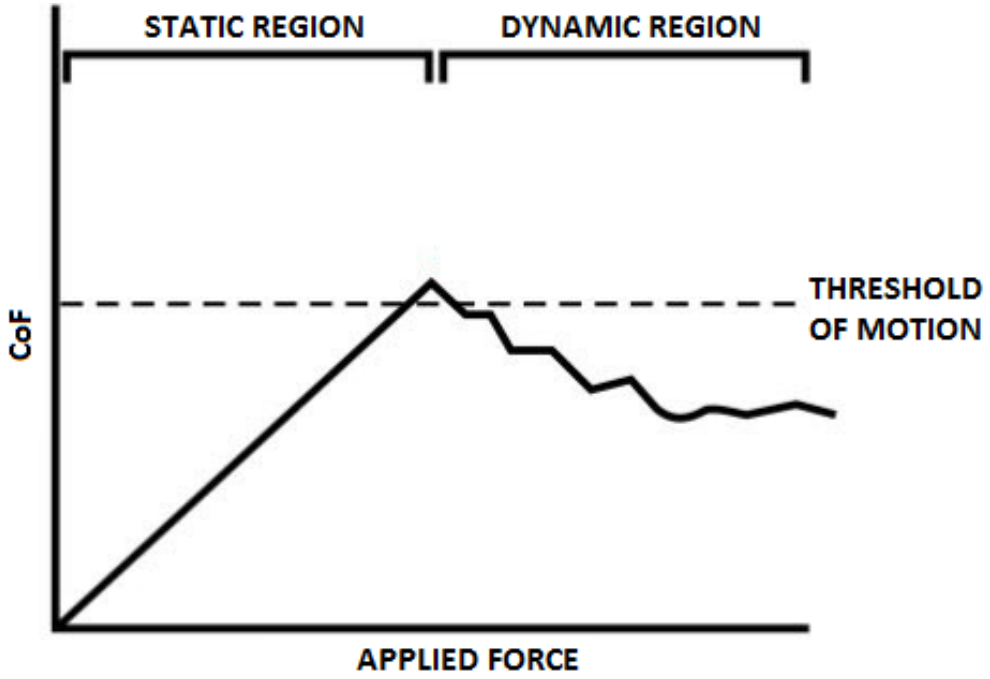

Figure 1.10 – Schematic graph showing the CoF depending on applied force on a pulled object. The static and dynamic regions are indicated. Modified from figure in [17].

Friction between the PM and the filling machines is important to study and to keep low enough for preventing PM from getting stuck, stopping the filling process. It is also important not to have too high friction between the inside and the décor layers of the PM since this will prevent sliding during roll up and cause bouncing.[18]

2 Objectives

The main goal of this thesis is to improve the understanding of pattern transfer in the nip and the connection between the properties of PM and its surface texture. This will be done by analysing and mapping 3D surface structures of CR and PM for both inside and décor polymer layers, and correlating them to functional properties defining the performance of finalised product, such as properties related to appearance and friction.

For the inside layer, two CR surfaces manufactured with the same specifications will be studied. One of them was treated by an additional chrome layer before delivery and implementation into the lamination process, which resulted in a deviation of the performance of the PM.

In the décor layer case, one CR surface and corresponding PM surfaces will be studied. This side of the PM has properties deviating from the inside cases.

Adding to the main part, appearance and friction measurements will be performed on inside and décor PM surfaces to see how they are influenced by the surface texture of the PM. An already tested method for friction measurements on PM surfaces using a tensile testing device will be used.

The questions that need to be answered are:

- What is a qualitative difference between CR and PM of the two inside CR-PM pairs?
- How much of an ideal negative is received in the pattern transfer from CR to PM? This is to be judged by analysing 3D surface parameters for the two inside CR-PM pairs separately.
- Is it possible to see this difference by analysing the 3D surface parameters? Can it be related to different performance properties for respective PMs?
- What difference is seen when comparing inside and décor layers?

Therefore, this thesis has the following objectives:

- To carry out a literature survey for finding best practices in unraveling a relationship between 3D surface parameters and pattern transfer in a lamination process.
- To analyse surface textures of CR replica sample surfaces and PM surfaces, inside/décor layers, using a 3D microscopy technique.
- To identify correlations between aforementioned findings and the performance (appearance and friction) of PMs.

3 Experiments

Both sides of the PM were analysed, *i.e.* the inside and the décor polymer layers. This section explains how the samples were prepared and examined in a microscope, and how respective data were compiled for further analysis. In the end of this section, the description of methods used to measure the properties of samples are presented.

3.1 Analysis of inside and décor PM surfaces

In Table 3.1, all the studied samples are listed and labeled.

Table 3.1 – Samples studied in this project.

Side	Type	Sample name
Inside	PM	ins_PM_1
		ins_PM_2
		ins_PM_3
		ins_PM_4
	CR	ins_CR_1
		ins_CR_2
Décor	PM	dec_PM_1
		dec_PM_2
		dec_PM_3
		dec_PM_4
	CR	dec_CR

For the inside PM layer, four samples were selected and cut out from PM rolls in duplicates, making it eight inside PM samples in total. Three of the PM duplicate pairs, named ins_PM_1, ins_PM_3 and ins_PM_4, were patterned by similar CRs giving them well-desired functional properties in terms of glossiness and friction, but the patterning took place at two different factories. The last duplicate pair, called ins_PM_2, was patterned by a different CR giving functional properties undesired to the specific PM type, specifically, a surface with excessively high friction.

Samples ins_PM_1 and ins_PM_2, and their corresponding CR surfaces, are used in a comparative analysis between CR and PM samples. This is reported in Section 4.1.

The CR surfaces were studied by using replica kits already cast from respective surfaces. Using the replica kit instead of a direct testing on CR

surface is a verified method at Tetra Pak, which enables all CR measurements to be performed in the same environment as in the PM cases.

The second experimental study was focused on the décor polymer layer. Four PM samples, named dec_PM_1, dec_PM_2, dec_PM_3 and dec_PM_4, were cut out in duplicates from the same PM rolls as in the study of the inside polymer layer.

In both inside and décor studies, the PM samples were coated with gold and then studied together with the corresponding CR replica kits in a 3D microscope, as described below. Quantitative surface characteristics from the microscope were exported for further processing and statistical analysis.

3.1.1 PM sample preparation

The principle of focus variation microscopy demands that PM samples had to be coated with a thin metal layer for observations to make possible finding the focus on otherwise transparent polymer surface. This was done by sputtering gold onto the PM samples and thus creating a thin layer of gold on top of the outermost polymer layer of the PM. The procedure was carried out using a designated sputter apparatus (JEOL JFC-1300) with a chamber containing a disc made of gold in the top, a sample holder in the bottom, a vacuum pump enabling pressures down to a few Pa and an Ar gas tube to enable purging of the enclosed chamber. The setup is shown in Figure 3.1.

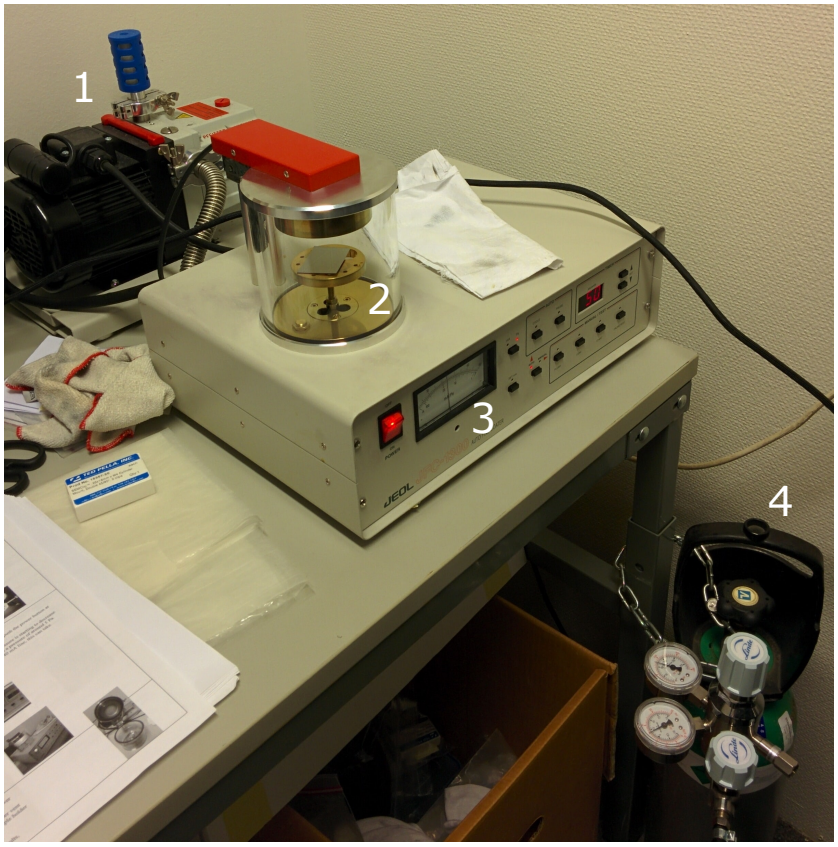

Figure 3.1 – gold sputter setup when in use. In the picture: 1. Vacuum pump, 2. Sample holder with PM sample, 3. Instrument panel of gold sputter, 4. Ar gas tube.

For one procedure, a PM sample was put on the sample holder in the chamber and the lid of the chamber was shut. The vacuum pump was then turned on and evacuating the chamber began. After the pressure decreased to a suitable value (5 Pa), a sputtering cycle was initiated, where the chamber was purged with Ar gas two times, after which a bias was built up in the chamber between the sample holder and the disc. When the bias was high enough, a plasma of Ar ions was created. The high kinetic energy of Ar ions enabled gold atoms to be sputtered off the surface of the disc and deposited onto the PM sample. After a certain time (50 s), the bias was cut off and the cycle was finished leaving a layer of gold less than 20 nm thick deposited on the top of the PM sample. In Figure 3.2a the sample is seen inside the chamber when the plasma is on, and in 3.2b a finished gold plated sample is shown. Both images show gold plating of an inside PM sample.

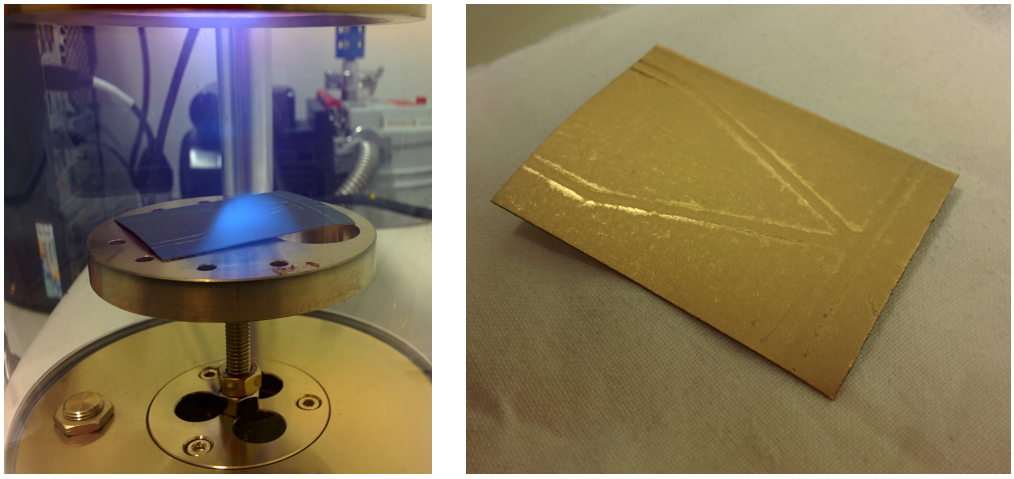

(a) **(b)**

Figure 3.2 – (a) Sample inside the chamber when plasma is on and (b) the finished gold plated sample.

3.1.2 Analysis of surface texture

The textures of PM and CR surfaces were studied using an Alicona IF Portable 3D microscope. This instrument uses a focus variation technique to create an image. The microscope is not equipped with a sample holder, which means a sample should be placed in the optical axis of the microscope below objective on any surface within the range of focus variation accessible by the instrument. This set up in combination with portability of the microscope allows measurements of surfaces in their working environments. The microscope generates a 3D image like the one seen in Figure 3.3.

Figure 3.3 – 3D image of inside PM surface generated by the Alicona IF Portable.

For each studied specimen (PM or CR), the measurements were performed in nine unique positions collecting data from a 3x3 pattern. Each position was examined using three different magnifications, 5x, 10x and 20x. This means that the data of surface texture was collected 27 times for each specimen. Note that the actual surface of the replica kit, *i.e.* the negative of the CR surface, was studied in the microscope.

It should also be noted that a roughness filter was used in evaluating parameters, so that all long wavelength components were filtered out in the analysis.

3.1.3 Post-processing and statistical analysis of surface texture

The collected data on quantitative surface texture characteristics were separated into three sets corresponding to the parameter groups described in detail in Section 1.3.

MATLAB was used to handle the data and to create diagrams for comparison. Each parameter set was formatted to remove outliers, and bullet diagrams for each sample were created. PM to CR samples at 20x magnification were found most representative for comparison, which allowed investigating trends and differences in mean values with 95% confidence interval.

3.2 Parameter analysis

When analysing the aforementioned statistical parameters, the means and the 95% confidence intervals were examined. If the intervals do not overlap, the samples are said to have a statistically significant difference in that parameter. A selection of parameters was made based on such a significance and a correlation in the trend of mean values for a specific parameter with a proposed hypothesis. Such an analysis was carried out for all the parameters of all the specimen surfaces.

3.3 Property studies

3.3.1 Gloss

The gloss of different PM samples was classified by ocular inspection as high or low. Respective images were taken by simply placing the samples on a white underlay and capturing photos of them when illuminated by camera flash. This ocular inspection was then compared to the parameters gathered from microscopy to see if any correlations can be found.

3.3.2 Friction

Friction was measured for three representative samples, ins_PM_1, ins_PM_2 and dec_PM_2. This was done using an Instron 5566 friction measurement device and following a method used and verified at Tetra Pak. A metal sled weighing approximately 200g was dragged along the surface of the three samples, and friction force was recorded, see setup in Figure 3.4. The sled was dragged 100 mm each time, and this operation was performed three times for each sample. The absolute values of the friction measurements are not important for this work. Therefore, the PM samples were ranked based on relative comparison between them. These rankings were then compared to the other parameters studied to examine the existence of any correlations.

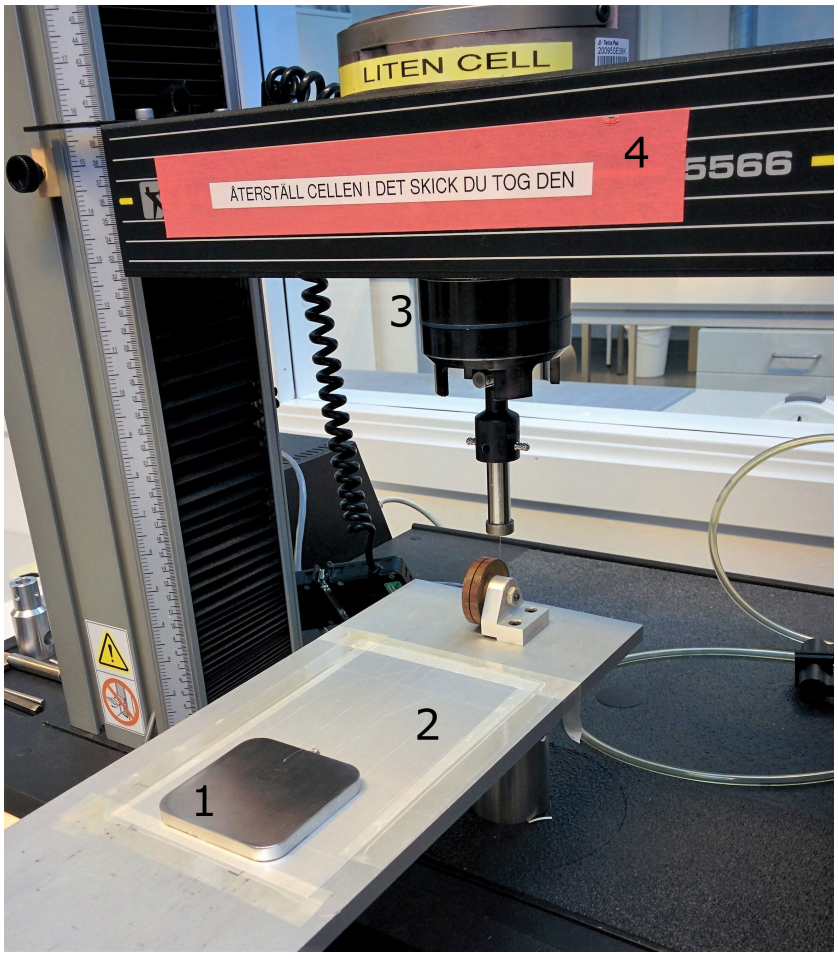

Figure 3.4 – Setup for friction analysis. 1. Sled, 2. Inside PM sample surface, 3. Load cell, 4. Crosshead.

4 Results and Discussion

4.1 Inside PM surfaces

In this section, the data from the inside polymer layer of the PM will be analysed in terms of surface texture characterisation of gold plated actual PM surfaces and replica kits cast from corresponding CR surfaces. In particular, a comparison of the two different CR surfaces and defined PM surfaces is given using visual images and selected diagrams produced from the compiled data.

4.1.1 Qualitative visual analysis

The first results received in the Alicona instrument were true and pseudo colour images of the surfaces under scrutiny. Figure 4.1 presents the comparison of true vs pseudo colour images at 20x magnification of samples ins_CR_1 and ins_PM_1. The CR surface shown in Figure 4.1a consists of randomly sized and shaped surface features. The surface height varies between -5 and +2 μm, as can be found in Figure 4.1b. The colour of the true image in Figure 4.1a is red, which comes from the colour of a resin in the replica kit. It should be noted that the location of CR surface in Figure 4.1a,b does not correspond to the roll area defining PM texture in Figure 4.1c,d. In Figure 4.1c, the brown-gold colour of the polymer sheet originates from the colour of the gold layer deposited on the top of PM surface. Comparing Figures 4.1a and c, the surfaces seem to have similar randomly sized and shaped features, indicating that the PM surface looks like it is a negative of the CR surface. Nevertheless, detailed analysis of the pseudo images in Figures 4.1b and d reveals that the PM surface is more rough having a bigger height distribution.

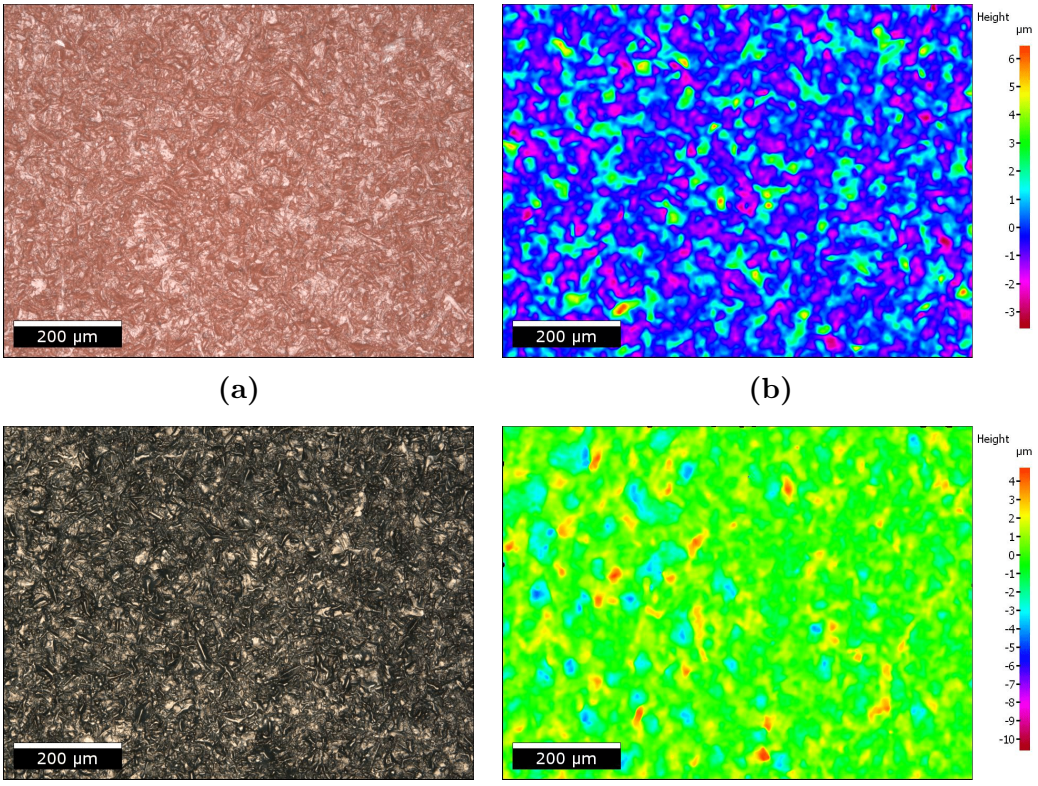

Figure 4.1 – True and pseudo coloured images for the ins_CR_1 (a-b) and ins_PM_1 (c-d) surfaces.

The surfaces for samples ins_CR_2 and ins_PM_2 are seen in true and pseudo colours in Figure 4.2. Their visual characteristics are not the same as in the first CR-PM pair. The surface in Figures 4.2a,b consists of a bubble-shaped landscape with similar height differences as the first CR surface. Similar to the case in Figure 4.1, the PM surface in Figures 4.2c,d appears to be somewhat a negative of its CR counterpart in Figures 4.2a,b, while the PM surface has wider variation of feature heights.

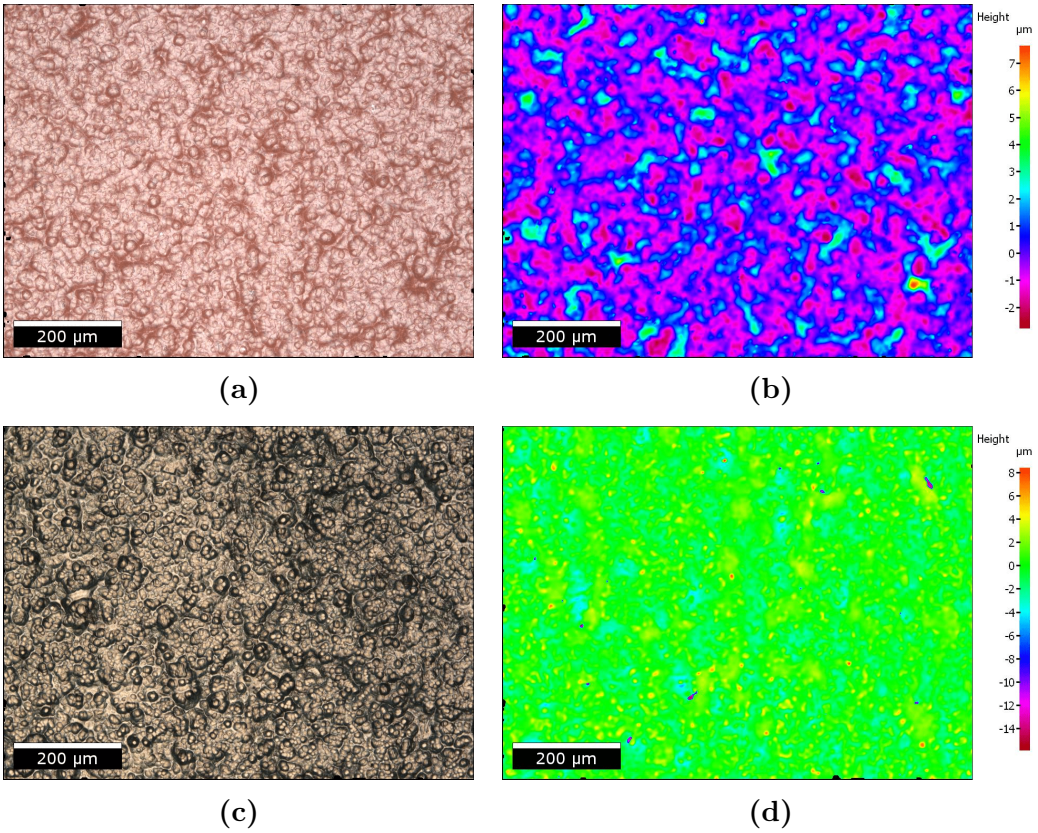

Figure 4.2 – True and pseudo coloured images for the ins_CR_2 (a-b) and ins_PM_2 (c-d) surfaces.

A reason for the bubble-like landscape of the ins_CR_2 surface (and consequently its PM counterpart) is the event of nucleation growth. This growth took place in the fabrication process of the CR, in a stage that is additional to what was performed when fabricating ins_CR_1. In that stage, the sharp edges seen on ins_CR_1 function as nucleation centers, and hemispheres, or bubbles, subsequently grow out from them.

In Figure A.1 in the appendix, true and pseudo coloured images of ins_PM_3 and ins_PM_4 are shown. They both show the same kind of characteristics as ins_PM_1.

4.1.2 Analysis of 3D surface parameters

In diagrams shown below, all individual measurements are represented by either grey bullets or red asterisks, while the average of each data set is indicated by a blue bullet. Note, the red asterisks represent outlier values that were not taken into account in the statistical analysis of the data. The

outliers are discussed in detail in Section 4.4. 95% confidence intervals are also calculated and presented in the diagrams by black lines.

Root mean square roughness $\mathbf{S_q}$ is shown in Figure 4.3. It shows that the PMs have rougher surfaces compared to the master CRs. This observation is further supported by $\mathbf{S_{10z}}$ diagram shown in Figure 4.4. For both parameters, the difference is larger between ins_CR_2 and ins_PM_2 compared to ins_CR_1 and ins_PM_1. It means that a greater increase in roughness is created during the transfer of pattern from the bubble-like landscaped CR to the respective PM.

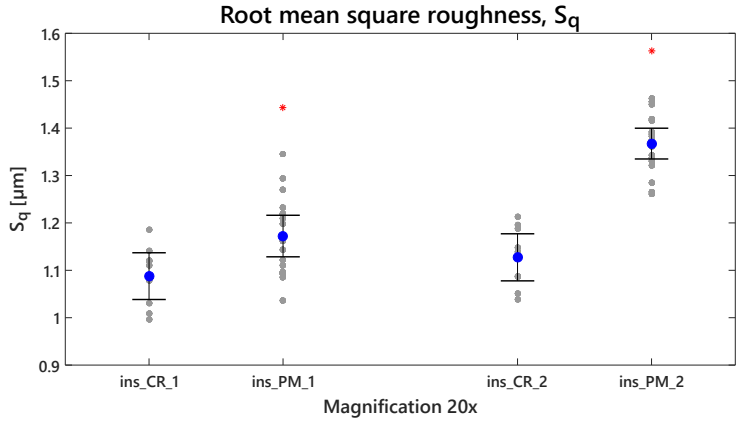

Figure 4.3 – Root mean square roughness data of ins_CR_1 and ins_CR_2 surfaces and respective PMs.

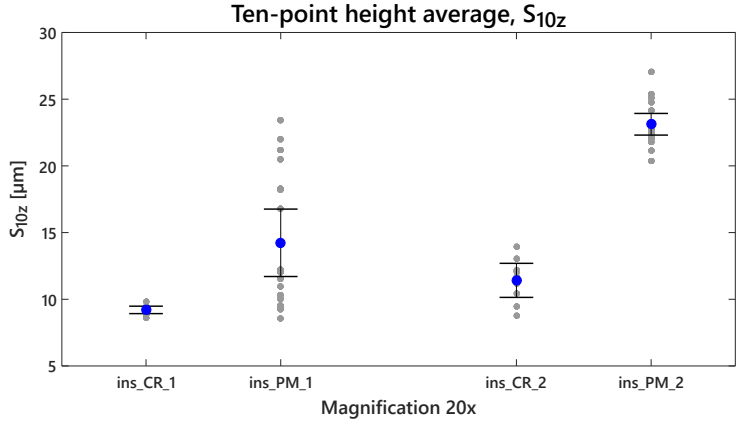

Figure 4.4 – Ten-point height average of ins_CR_1 and ins_CR_2 surfaces and respective PMs.

Maximum peak height $\mathbf{S_p}$ is shown in Figure 4.5. One of the samples in each CR-PM pair has a large interval, which reaches into the corresponding

sample interval in that pair. This means that similar maximum peak heights will be transferred when the PM is defined.

In the case of maximum valley depth $\mathbf{S_v}$, shown in Figure 4.6, a more general trend is found between the two CR-PM pairs. Both the defined PM surfaces get deeper valleys compared to their master CRs, respectively. This varies from the observations in the $\mathbf{S_p}$ case. ins_PM_1, with its sharp grained and randomly distributed surface, has a rather wide spread of values, giving it a wide interval. The variation of both PMs are higher than that in corresponding CRs.

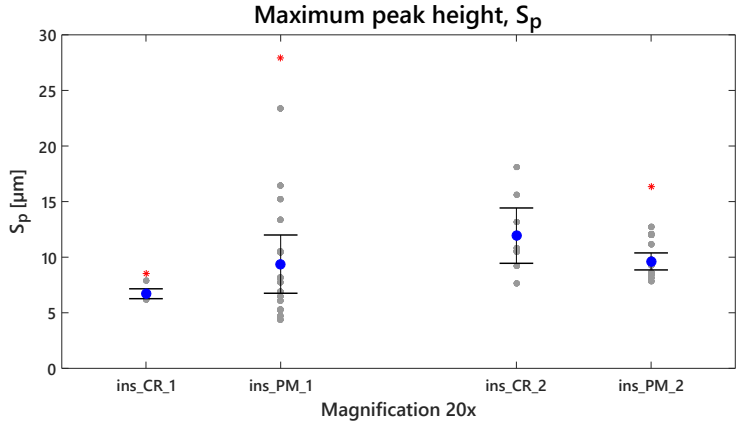

Figure 4.5 – Maximum peak height of ins_CR_1 and ins_CR_2 surfaces and respective PMs.

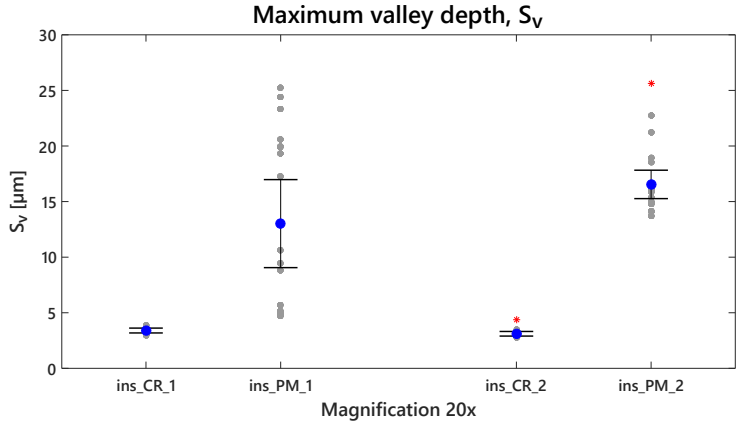

Figure 4.6 – Maximum valley depth of ins_CR_1 and ins_CR_2 surfaces and respective PMs.

The skewness $\mathbf{S_{sk}}$ of CR and PM surfaces are shown in Figure 4.7. The CR surface means are positive, which implies that they have a texture dominated

by peaks. The mean $\mathbf{S_{sk}}$ values of PM surfaces are close to 0, which indicates that the surface is less dominated by peaks or valleys, *i.e.* the surfaces are more symmetric. This is consistent with the $\mathbf{S_p}$ and $\mathbf{S_v}$ parameters, where increased maximum valley depths on the PM act as counter weight and balance the skewness.

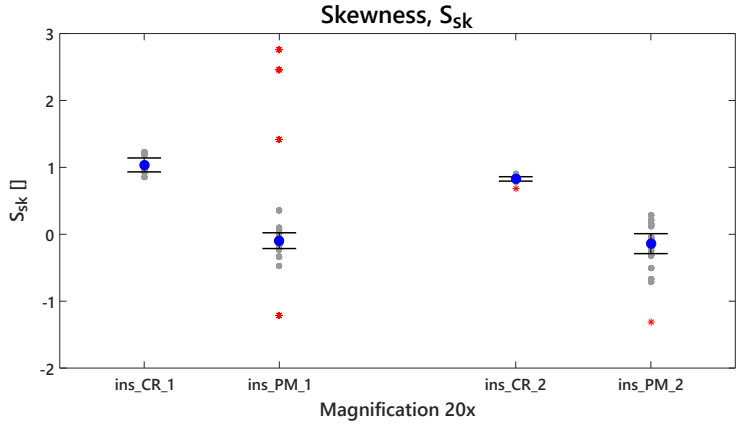

Figure 4.7 – Skewness data for ins_CR_1 and ins_CR_2 surfaces and subsequently defined PM counterparts.

The results reported in Figures 4.3-4.7 indicate that the PM becomes rougher compared to its master CR. The same results also indicate that the PM has similar maximum peak heights, receive deeper valleys and get a more symmetric surface. The most probable reason for this is the trapping of air when the PM is pressed against the CR. This affects liquid polymer creating more valleys on solidified PM surface. Thus, it becomes more rough and symmetric compared to the peak-dominated CR surface.

Reduced valley depth $\mathbf{S_{vk}}$ is shown in Figure 4.8. The mean values of $\mathbf{S_{vk}}$ are higher in PMs, which suggests that, in the pattern transfer of both PMs, deeper valleys are created on PM surface compared to respective master CR. This observation is consistent with previous diagrams, while also strengthening the hypothesis of the presence of air in the process. The same can be seen for $\mathbf{V_{vv}}$ in Figure 4.9, where a bigger void volume is produced on PM surfaces than on CR counterparts.

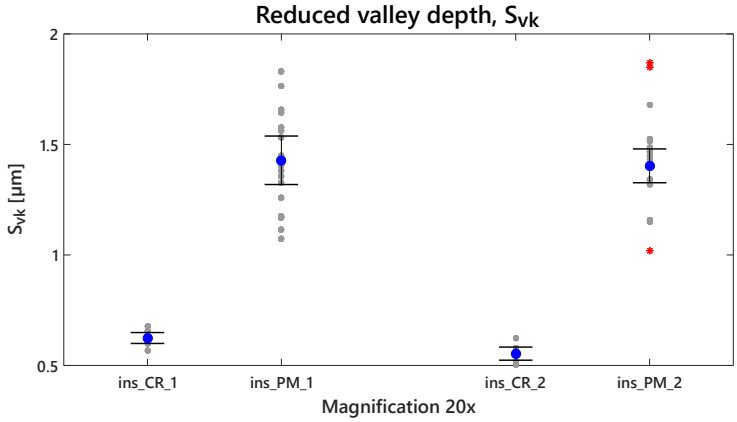

Figure 4.8 – Reduced valley depth on ins_CR_1 and ins_CR_2 surfaces and subsequently defined PM counterparts.

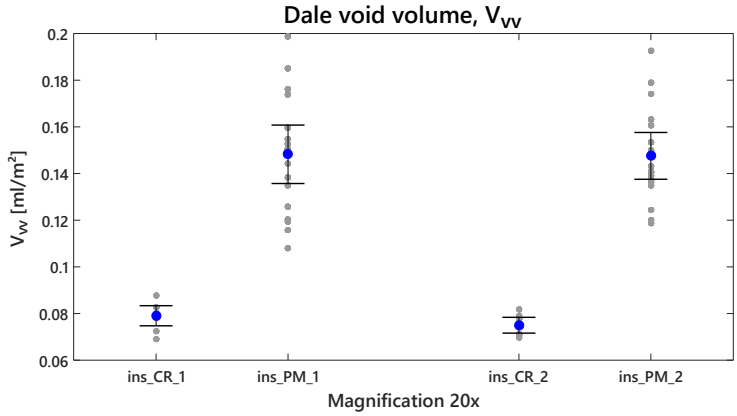

Figure 4.9 – Dale void volume on ins_CR_1 and ins_CR_2 surfaces and subsequently defined PM counterparts.

Kurtosis $\mathbf{S_{ku}}$ is shown in Figure 4.10 for the comparison between CR and PM surfaces in the two sample pairs. PMs show wider intervals and higher mean values that indicate the formation of a sharper surface.

It is worth stressing again that $\mathbf{S_{sk}}$ and $\mathbf{S_{ku}}$ parameters have higher order powers in their equations, which means that they are prone to give faster error propagations than other parameters. Thus, they require more measurements to provide values with higher statistical significance.

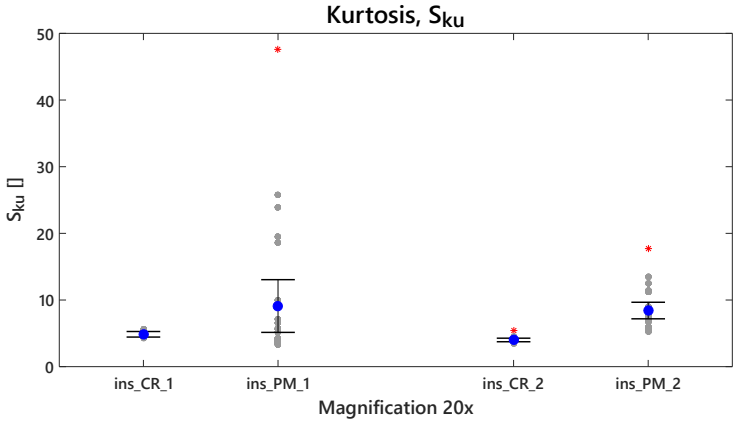

Figure 4.10 – Kurtosis on ins_CR_1 and ins_CR_2 surfaces and subsequently defined PM counterparts.

The root mean square surface slope $\mathbf{S_{dq}}$ is shown in Figure 4.11. Indicating that from ins_CR_1, the same $\mathbf{S_{dq}}$ is produced on ins_PM_1. Along with the fact that $\mathbf{S_q}$ increases from CR to PM (Figure 4.3), this suggests that the features on ins_PM_1 will be more smeared than those on master CR counterparts. In the second CR-PM pair, higher $\mathbf{S_{dq}}$ is produced on the ins_PM_2. Due to the difference in $\mathbf{S_q}$ parameter, it is difficult to come to similar conclusions in this pattern transfer.

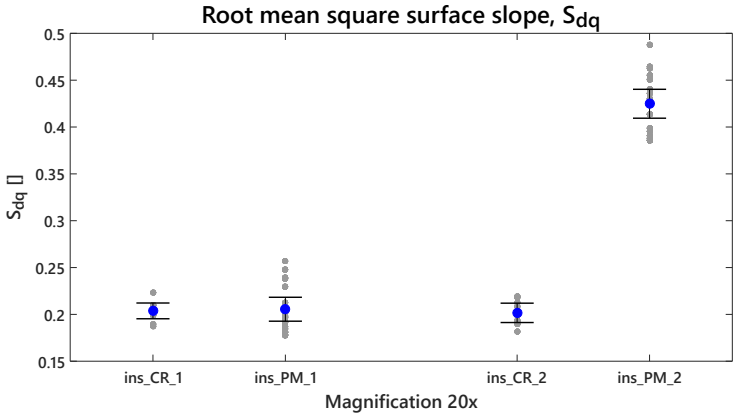

Figure 4.11 – Root mean square surface slope on ins_CR_1 and ins_CR_2 surfaces and subsequently defined PM counterparts.

Further parameters presented in Appendix A contribute to a more thorough characterisation of surfaces, but are irrelevant to the given hypothesis.

4.2 Décor PM surfaces

In this section, the data from décor, or outside, polymer layer of several PM samples will be compared to a CR replica kit surface. Note, all PM samples were defined by CRs produced with the same specifications and, hence, all show similar surfaces. Therefore, only one PM sample (dec_PM_4) is used in the following comparison between CR and PM in Figures 4.12 and 4.13.

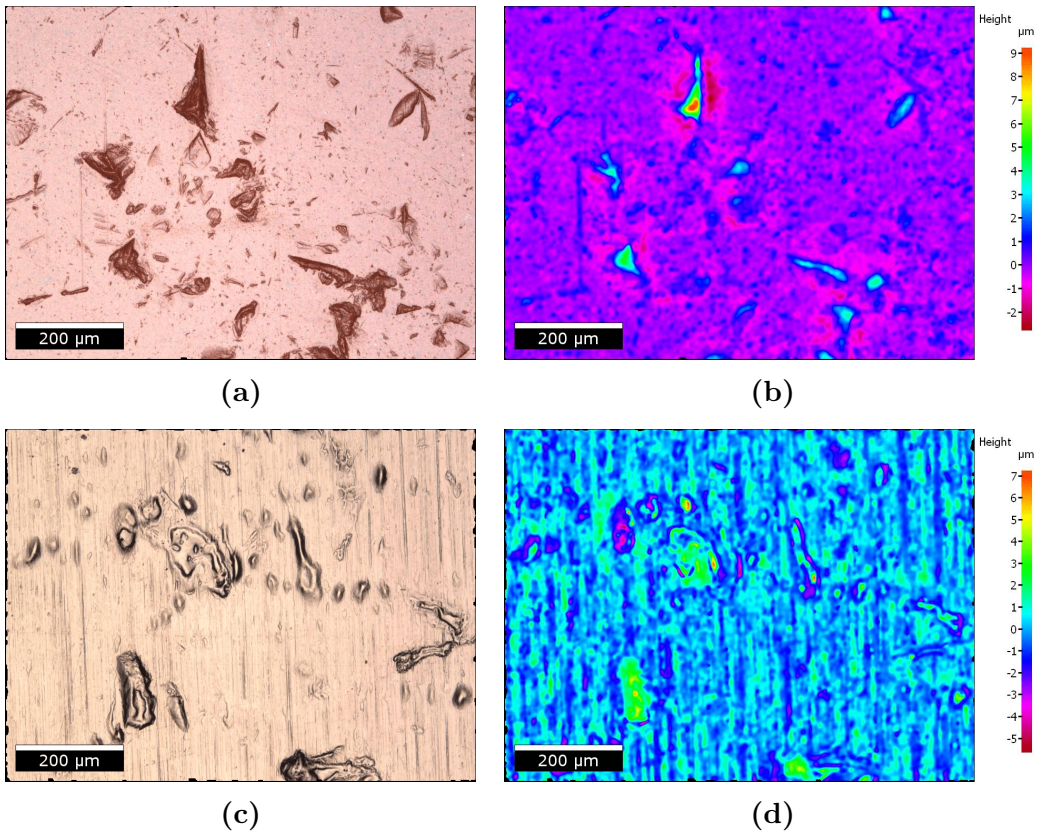

Figure 4.12 – True and pseudo coloured images for dec_CR (a-b) and dec_PM_4 (c-d) surfaces.

When looking at the true colour images in Figure 4.12, scattered structures on the otherwise flat surfaces are clearly seen. They are bigger than those seen on the inside samples. The analysis of these structure formations suggest that in this case the CR is sand blasted with bigger, but fewer, sand grains than were used in processing the inside CRs.

In the dec_PM_4 images, smaller vertical linear features are seen. They are called grinding marks. These features result from the polishing step in the fabrication process of CR that defined dec_PM_4. The sand blasting step

would have been done after the polishing step. This explains why no grinding marks are seen on the bigger structures on the PM surface. Since the grinding marks are not found in the dec_CR case, it should be noted that dec_CR is not the exact one used to define dec_PM_4. The polishing step was skipped when producing dec_CR as the result of the surface already being flat enough after the chroming step. This could be a difference between CR suppliers, or even between different CRs from the same supplier. Nevertheless, dec_CR is still a décor layer CR and, hence, it is considered relevant to use its images in the following comparisons between CR and PM surfaces. Looking at the gradient distribution of these surfaces, presented in Figure 4.13, a clear repeating shape is seen in the PM but not in the CR case.

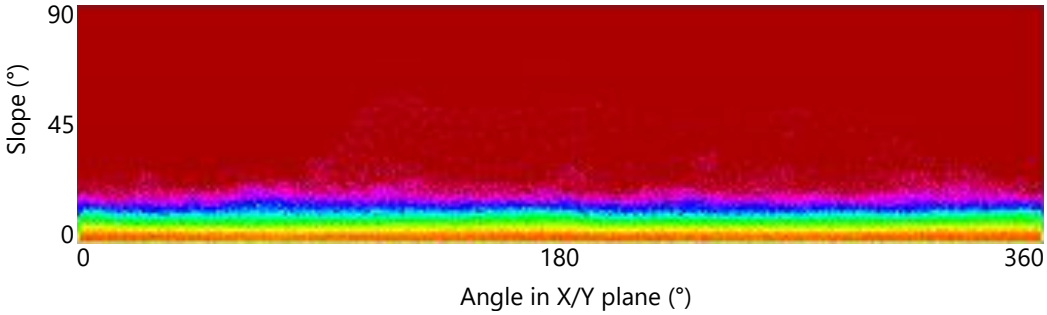

(a)

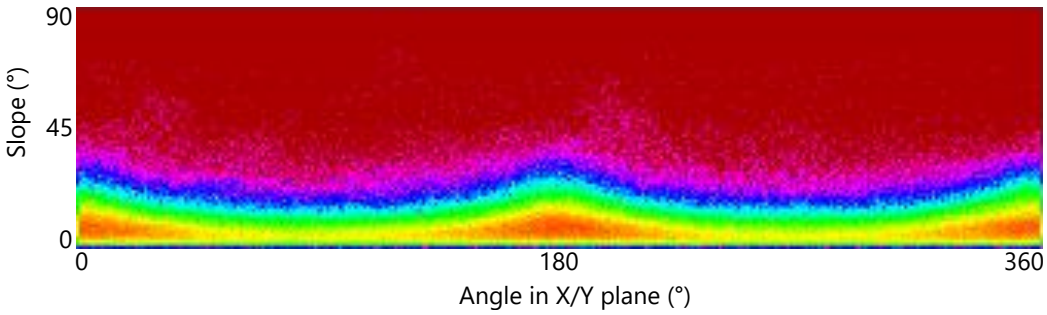

(b)

Figure 4.13 – Images of the gradient distribution of dec_CR (a) and dec_PM_4 (b) surfaces.

The data from Figure 4.13 for some of the samples is presented in Figure 4.14. Most of the samples show the spread in angles of more than 30 degrees. All the décor PM samples show similar trends as dec_PM_1, seen in Figure 4.14, with the spread of less than 10 degrees. This indicates that the décor layer has a preferred direction as can be seen from the grinding marks in Figures 4.12c and d. These marks are not visible on any of the inside sam-

ples, and can explain why they do not show the same trend for a preferred direction.

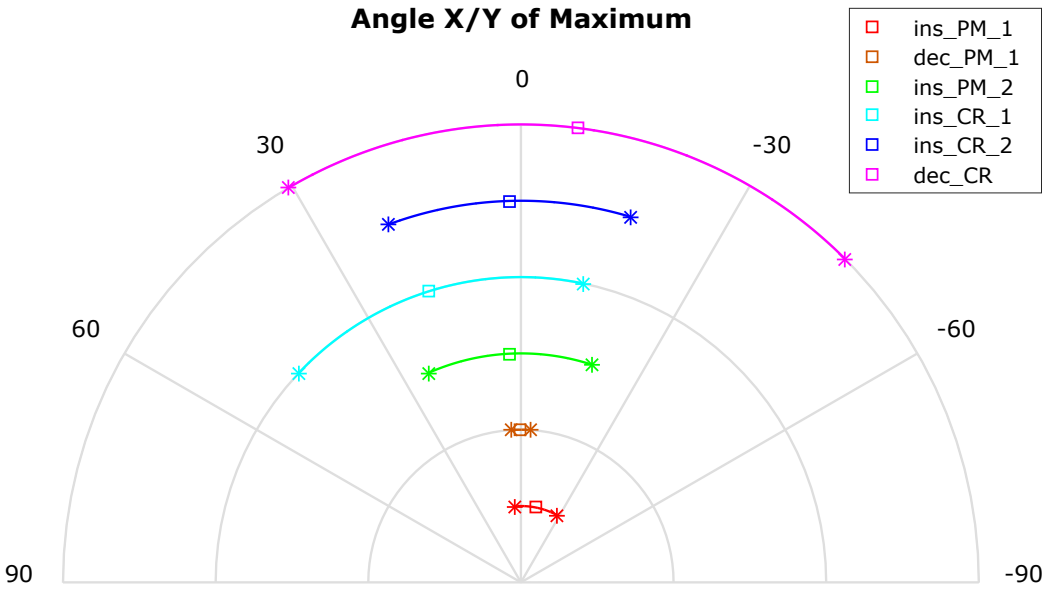

Figure 4.14 – Mean and 95% confidence interval for the angle X/Y of maximum for some of the samples.

On some of the studied PM samples, distinct scratches are seen on the surfaces. One example of such a feature is seen in the true coloured image in Figure 4.15. These errors are the results of wear on the CR surface that was used to define the PM texture. In the pseudo coloured image, the scratches can be seen, but they are less visible. They tend to show only a minor height difference compared to the otherwise flat surface. In the gradient distribution, it is not possible to identify anything that would indicate the presence of scratches.

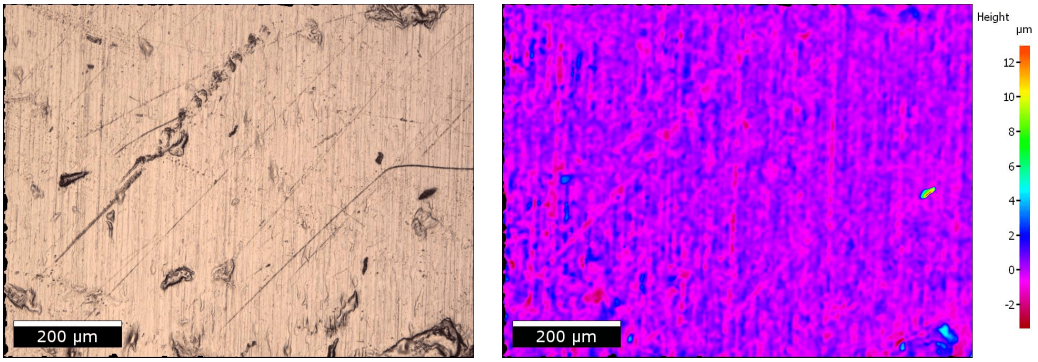

(a) **(b)**

Figure 4.15 – Images of the décor PM surface showing clear diagonal scratches. Looking carefully, the scratches are visible in the pseudo coloured images as well.

Another interesting observation made in this study is the white dots shown in Figure 4.16. This pattern was only seen on sample dec_PM_1. The origin of these dots is not determined. This is certainly not the artefact of gold plating stage in specimen preparation, since the non-gold plated sample measurements show the same dots (it was possible to do measurements of the polymer surface on the décor side in 10x magnifications without having the samples gold plated). As a hypothesis, there might be a thin holographic film laying below the polymer film that gives rise to the dots.

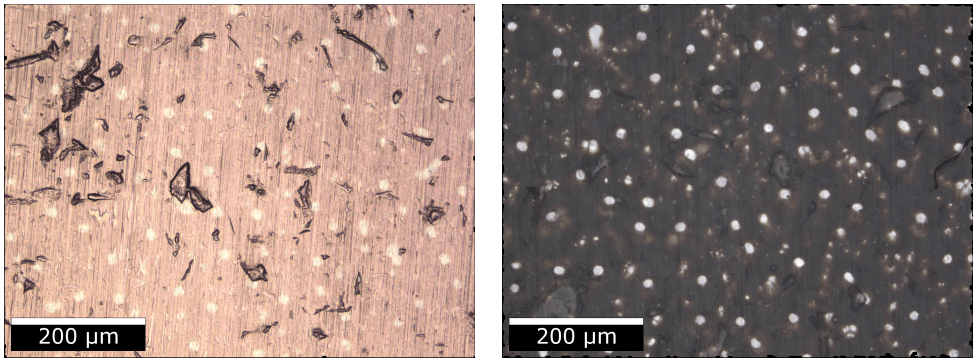

(a) **(b)**

Figure 4.16 – Images of the dec_PM_1 surface showing white dots. Gold plated in (a) and not gold plated in (b). Note that these images are taken at 10x magnification.

4.3 Properties of PM

In this section, the results from visual analysis and parameter study are correlated with the properties of both PM sides.

4.3.1 Gloss

In Figure 4.17, the two sample sides ins_PM_3 and dec_PM_3 are shown to visualise how the glossiness of the inside and décor layer differs. The inside layer (a) shows a matt appearance compared to the décor layer (b), which shows a higher gloss.

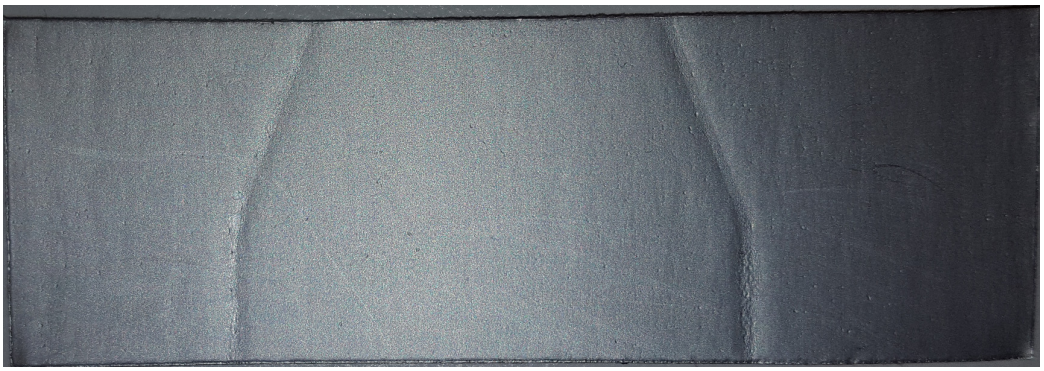

(a)

(b)

Figure 4.17 – Images of the ins_PM_3 (a) and dec_PM_3 (b) surfaces visualising a difference in glossiness.

The glossiness is related to the intensity of reflectance of light on a surface. Apart from being dependent on refractive index and the angle of incidence of the light, the glossiness is a factor of surface topography. As was seen in Section 1, Tetra Pak uses the same polymer for both inside and décor

layers, which means that the refractive index is the same for all samples. When visualising the glossiness, all the following images were taken from a similar angle, and hence the angle of incidence is considered constant. This means that the variation in glossiness should be due to a difference in surface texture.

As seen in Figure 4.17, the décor layer has a higher gloss. The micrographs of the two sides proved to show an obvious difference, where the inside layer surfaces, in general, consist of more densely packed features. This must mean that when light is shone on the surface, it will become scattered more, and glossiness will be lower than on the less densely structurised décor layer.

In Figure 4.16, white dots are seen on dec_PM_1. For further comparison, this surface is compared to dec_PM_3 in Figure 4.18. dec_PM_1 surface in (a) shows more dotted reflection compared to dec_PM_3 in (b), and glossiness on dec_PM_1 appears higher. The higher glossiness is not necessarily the result of a difference in surface topography between the samples, but can also be explained by the holographic film lying between the polymer and the paperboard on dec_PM_1.

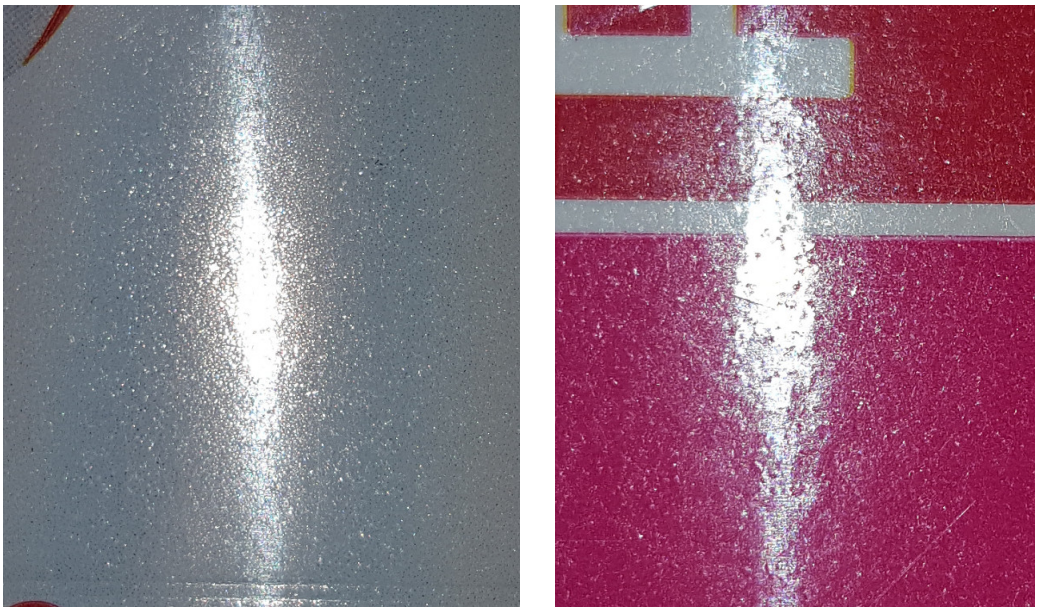

(a) **(b)**

Figure 4.18 – Images of the dec_PM_1 (a) and the dec_PM_3 (b) surfaces to visualise difference in glossiness.

When comparing the parameter diagrams for the inside and the décor, nine parameters are found to demonstrate difference between the surfaces and to explain difference in gloss. These parameters are $\mathbf{S_a}$, $\mathbf{S_q}$, $\mathbf{S_k}$, $\mathbf{S_{pk}}$, $\mathbf{S_{vk}}$, $\mathbf{V_{mc}}$, $\mathbf{V_{vc}}$, $\mathbf{V_{vv}}$ and **Angle X/Y of Maximum**. Most of the respective diagrams can be found in Appendix B. In order to determine more accurately how these parameters affect the gloss of PM, a more thorough study of the glossiness have to be carried out.

4.3.2 Friction

In Figure 4.19, dynamic and static CoFs are shown for samples ins_PM_1, ins_PM_2 and dec_PM_2 when measured against a metal surface. These diagrams present statistical values in the same way as the statistical parameter diagrams in Section 4.1.2. It is seen that ins_PM_1 has lower CoF for both cases, and that the two other samples show similar values. This is interesting since the 3D parameters are not showing resembling trends seen in the diagrams in Appendix B. Instead, ins_PM_2 generally has the highest parameter value of the three, ins_PM_1 displays values in between, and dec_PM_2 has the lowest values. This indicate that the CoF cannot be directly correlated to the statistical parameters investigated in this work. The difference in CoF can be attributed to the geometry of the surfaces. The smoother surface of dec_PM_2 compared to ins_PM_1 might make the contact area greater and thereby result in a higher CoF. In the case of the two inside samples, the spherical shapes on the surface of ins_PM_2 could mean that the resulting contact area (when the polymer is compressed by the weight of the sled) is bigger than for the sharp features on ins_PM_1, causing an increased CoF.

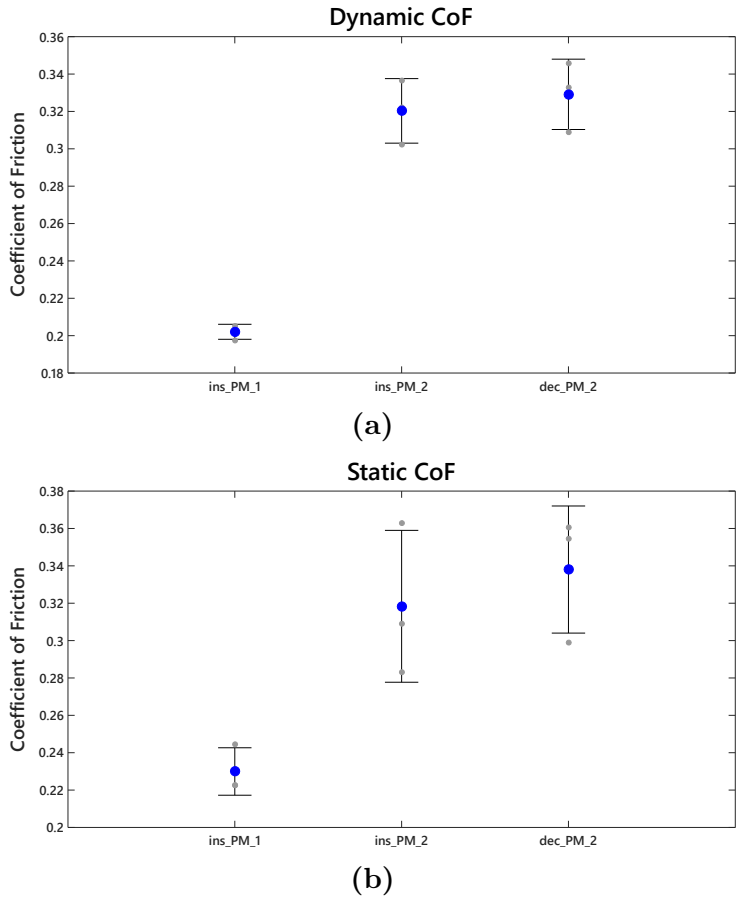

Figure 4.19 – Dynamic (a) and static (b) CoF for three PM samples measured against a metal surface.

4.4 Outlier analysis

When studying images of measured surfaces, several strange features are revealed. These features result in outliers in the parameter diagrams. In this section, some outliers will be re-visited and scrutinised. The outliers are evaluated using a script written in MATLAB and are indicated in red in the respective parameter diagrams in Section 4.1.2.

In $\mathbf{S_{10z}}$, $\mathbf{V_{vv}}$ and $\mathbf{S_{dq}}$ parameter cases, all values remained when outliers were evaluated. Outliers were found for parameters $\mathbf{S_q}$, $\mathbf{S_p}$, $\mathbf{S_v}$, $\mathbf{S_{sk}}$, $\mathbf{S_{vk}}$ and $\mathbf{S_{ku}}$.

In the pseudo coloured image in Figure 4.20, a small, but very high, peak is apparent inside the yellow circle. A dark shadowy object can be observed inside corresponding yellow circle in the true coloured image. This is caused by dirt on the surface. If such features are present on the surface, this will

give rise to $\mathbf{S_p}$, $\mathbf{S_{sk}}$ and $\mathbf{S_{ku}}$ outliers. This verifies the instability of $\mathbf{S_{sk}}$ and $\mathbf{S_{ku}}$ parameters, resulting in deviating values due to present errors on the studied surface.

In Figure 4.21, three pink circles indicate small, but very deep, pits on the surface, and these features are found to be behind $\mathbf{S_v}$ outliers.

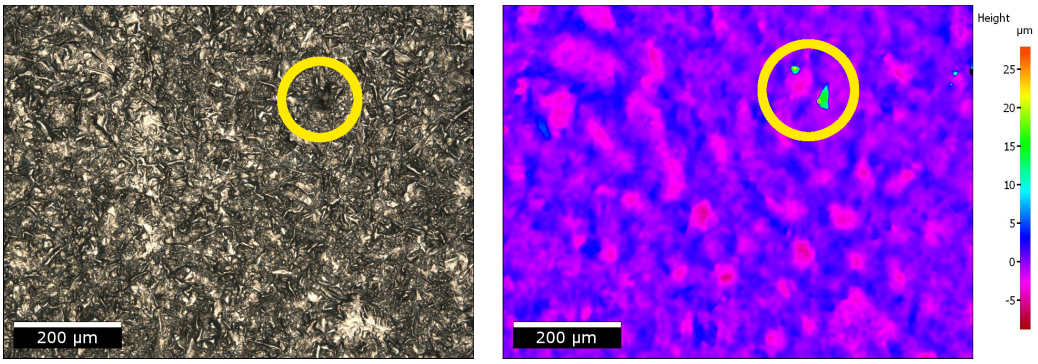

(a) **(b)**

Figure 4.20 – Images of a surface measurement giving an $\mathbf{S_p}$ outlier. The yellow circle indicates a very high peak.

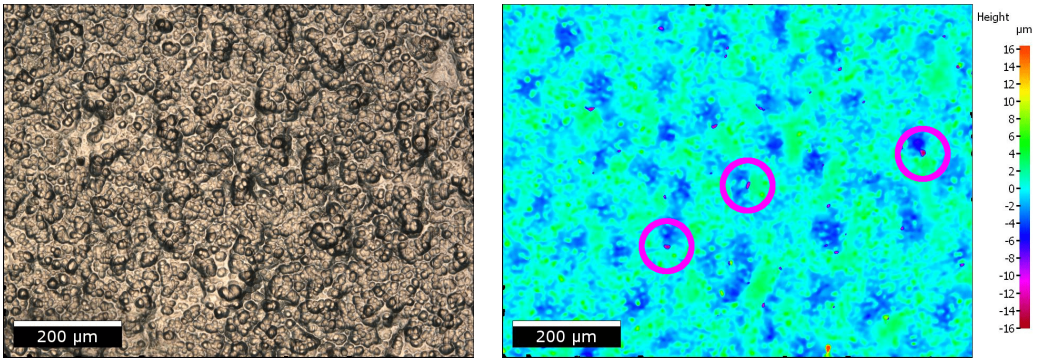

(a) **(b)**

Figure 4.21 – Images of a surface measurement giving an $\mathbf{S_v}$ outlier. Pink circles indicate very low valleys.

A bright plateau is seen inside the blue circle in Figure 4.22. A very small deep pit is seen inside the plateau in the pseudo coloured image, which is another source related to $\mathbf{S_{sk}}$ outliers.

In Figure 4.23, one high and one low point are identified. The true coloured image seems to have a dark round shaped object producing the

high peak. This object does not look the same as the one seen in Figure 4.20, being neither as high nor as sharp in its appearance. The shape of a pit in the middle of the image can be identified in the true coloured image by a shiny plateau highlighted by a blue circle. Both the identified features give rise to $\mathbf{S_{sk}}$ outliers.

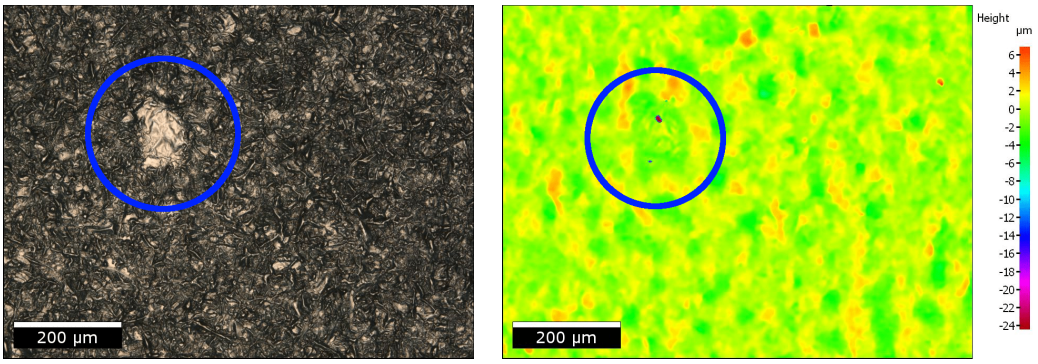

(a) **(b)**

Figure 4.22 – Images of a surface giving rise to an $\mathbf{S_{sk}}$ outlier. Blue circles indicate where the extremely low point is located.

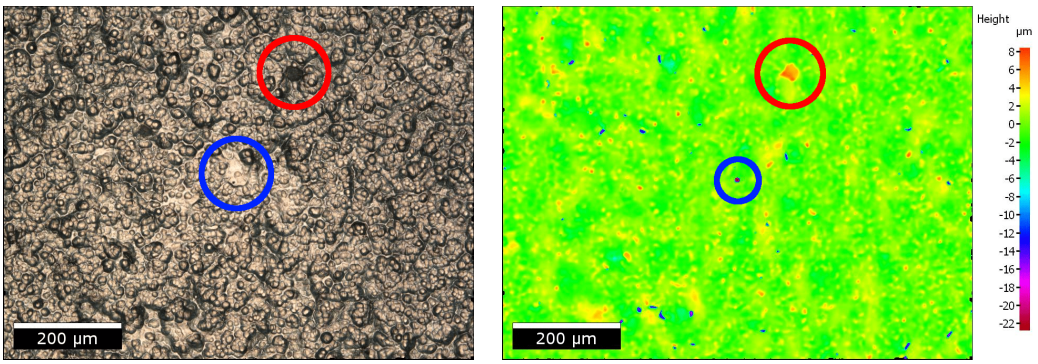

(a) **(b)**

Figure 4.23 – Images of a surface giving rise to an $\mathbf{S_{sk}}$ outlier. The red circle indicates high point and the blue, one of many scattered low points on the surface.

5 Conclusions

As described in the Objectives, the main goal of this work was to investigate the pattern transfer between CR and PM, *i.e* how close to a negative is received. In the inside PM layer pattern transfer, two different CR-PM pairs were analysed, where one CR defined PM surfaces with well-desired frictional behaviour and the other did not. The two CR surfaces appeared different in studied micrographs. An explanation was given that an additional processing step was performed on the CR producing PM with undesired friction, which made its surface having a bubble-like appearance. After studying the 3D surface parameter diagrams for the individual CR-PM pairs, a hypothesis about air affecting the molten polymer during the nip process is proposed based on the trends of mean values of the parameters. Therefore, the requirements for the inside PM pattern transfer is fulfilled. For the décor PM layer investigation, only one CR was studied and no obvious trends were found when comparing it to PM. Grinding marks seen on the PM samples were linked to an additional polishing step in the processing of the CR before it was sand blasted. Since no marks were seen on the CR analysed in this study, the CR and the PM samples could not be paired as in the inside PM study. To be able to draw conclusions about the pattern transfer for the décor PM layer, CR-PM pairs need to be analysed.

The next goal with this thesis was to intercorrelate surface textures of PM samples with their properties, in terms of glossiness and friction behaviour. For the glossiness study, images of illuminated PM samples were studied and compared to each other. Overall, the glossiness was higher for the décor layer, which is related to the less densely structured surfaces on the décor side that makes light scatter less. One décor PM sample had a more dotted appearance, both in glossiness study and in micrographs, and this was explained by a thin holographic film between the polymer layer and the paperboard in the PM.

For the friction study, a metal sled was dragged against PM surfaces to calculate the dynamic and static CoF. These coefficients were compared for three cases. One inside PM surface showed lower CoF values than both another inside PM surface and a décor PM surface. The two latter samples showed similar values. This somewhat confirms that the inside PM with high CoF had non-desired friction behaviour compared to the other.

When connecting the PM surface properties to the 3D parameters, the results showed different trends. Firstly, a set of parameter diagrams could indicate how the surface texture is related to the glossiness, but a more thorough study is needed to confirm those statements. Secondly, no parameters could be found to explain differences in friction behaviour.

6 Future work

To improve the understanding of pattern transfer in the nip and the connection between the properties of PM and its surface texture, the work done in this thesis needs to be continued. An investigation using more CR-PM pairs needs to be carried out in order to develop a transfer function for different parameters. The transfer function could then be used to study CR surface by just looking at the PM counterpart. This will simplify the studying of CRs by only having to send a PM sample for microscopic examination. An unnecessary travel to a factory for making a replica can then be excluded.

This investigation should then be complemented by investigating the connection between properties of interest, *e.g.* gloss and friction, and the surface parameters of PM materials. When these mechanisms are understood, a connection between PM properties and CR surface parameters can be made. After making this connection, it should be possible to choose the desired PM properties and obtain required CR parameters for sending to a supplier.

References

1. Coles, R. & Kirwan, M. *Food and Beverage Packaging Technology* 2nd. ISBN: 9781405189101 (Wiley-Blackwell, Chichester, UK, 2011).

2. *The History of Tetra Pak* (Accessed on 2017-02-16). <`http://www.tetrapak.com/about/history`>.

3. Rusnák, J. *et al.* Measurement of titanium surface roughness created by non-conventional cutting technology. *Res. Agr. Eng.* **57,** 57–60 (2011).

4. Blunt, L. & Jiang, X. *Advanced Techniques for Assesment Surface Topography* ISBN: 1903996112 (Kogan Page Science, Selwood Printing, West Sussex, U.K., 2003).

5. ISO. *Geometrical Product Specifications (GPS) - Indication of surface texture in technical product documentation* Standard ISO1302:2002 (International Organization for Standardization, 2002).

6. Stout, K. J. *et al. The Developement of Methods for the Characterisation of Roughness in Three Dimensions* ISBN: 0704413132 (European Comission, Brussels-Luxembourg, 1993).

7. ISO. *Geometrical product specification (GPS) – Surface texture, in Areal – Part 606: Nominal characteristics of non-contact (focus variation) instruments* Standard ISO25178-606:2015 (International Organization for Standardization, 2015).

8. Whitehouse, D. *Surfaces and Their Measurement* ISBN: 9781560329695. <`https://books.google.se/books?id=Q-oxVjI5-FUC`> (Taylor and Francis, 2002).

9. *Complete Guide to Surface Finish Charts, RA, RZ, Measurements, Callouts and Symbols* (Accessed on 2017-06-08). <http://www.cnccookbook.com/Calculators/SurfaceFinishChartMeasureSymbols.html>.

10. Jiang, X., Scott, P. J., Whitehouse, D. J. & Blunt, L. Paradigm shifts in surface metrology. Part I. Historical philosophy. *Proceedings of the Royal Society A* **463,** 2049–2070 (2007).

11. Leach, R. *Characterisation of Areal Surface Texture* ISBN: 9783642364570 (Springer Verlag, Berlin Heidelberg, 2013).

12. Danzl, R., Helmli, F. & Scherer, S. Focus Variation - a Robust Technology for High Resolution Optical 3D Surface Metrology. *Journal of Mechanical Engineering* **57,** 245–256 (2011).

13. Leach, R. *Optical Measurement of Surface Topography* ISBN: 9783642120114 (Springer Verlag, Berlin Heidelberg, 2011).

14. Leach, R. *Fundamental Principles of Engineering Nanometrology* ISBN: 9781455777501 (William Andrew Publishing, 2010).

15. *3D S parameters* (Accessed on 2017-03-21). <https://www.michmet.com/3d_s_parameters.htm>.

16. Silvennoinen, R., Peiponen, K.-E. & Muller, K. *Specular gloss* 1st ed. ISBN: 9780080453149 (Elsevier, 2008).

17. *Static vs Dynamic Friction* (Accessed on 2017-06-08). <https://www.blisterprevention.com.au/blister-blog/static-vs-dynamic-friction-reducing-the-shear-peak>.

18. Oros, S. *A Friction Model for Laminator Nips* eng. Student Paper. 2015.

Appendices

A Images and diagrams complementing the inside PM study

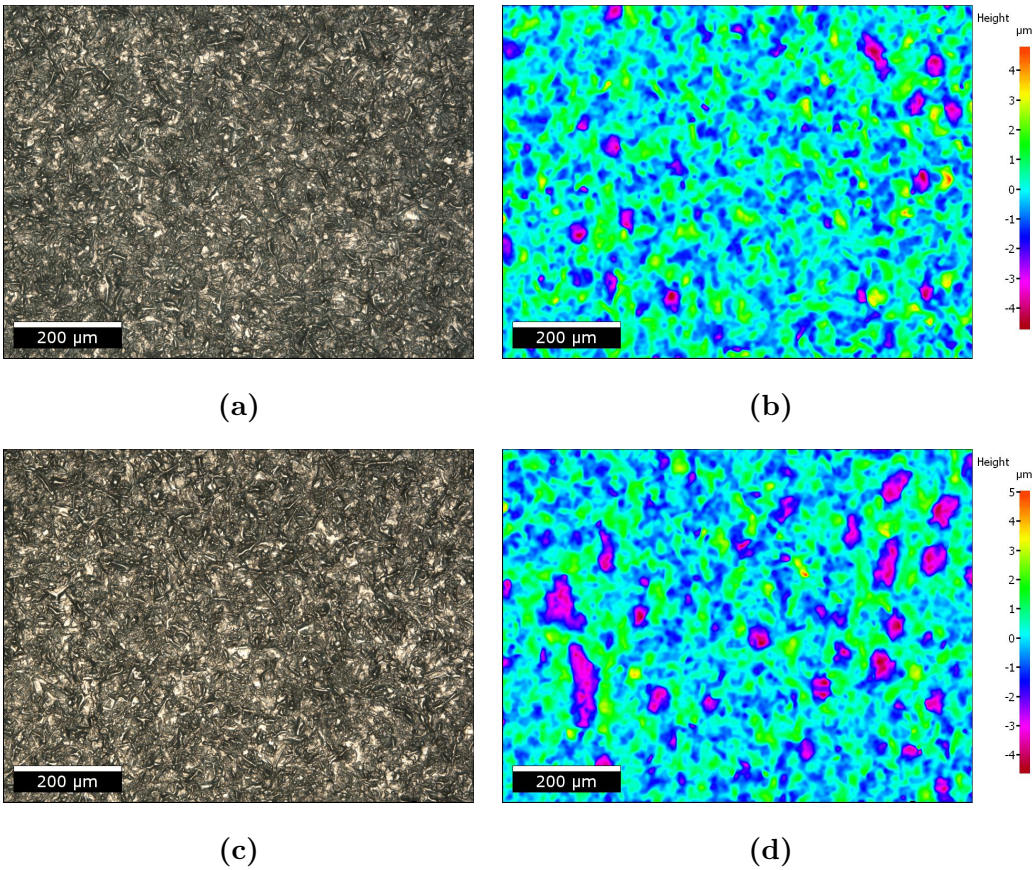

(a) **(b)**

(c) **(d)**

Figure A.1 – True and pseudo coloured images for the ins_PM_3 (a-b) and the ins_PM_4 (c-d) surfaces.

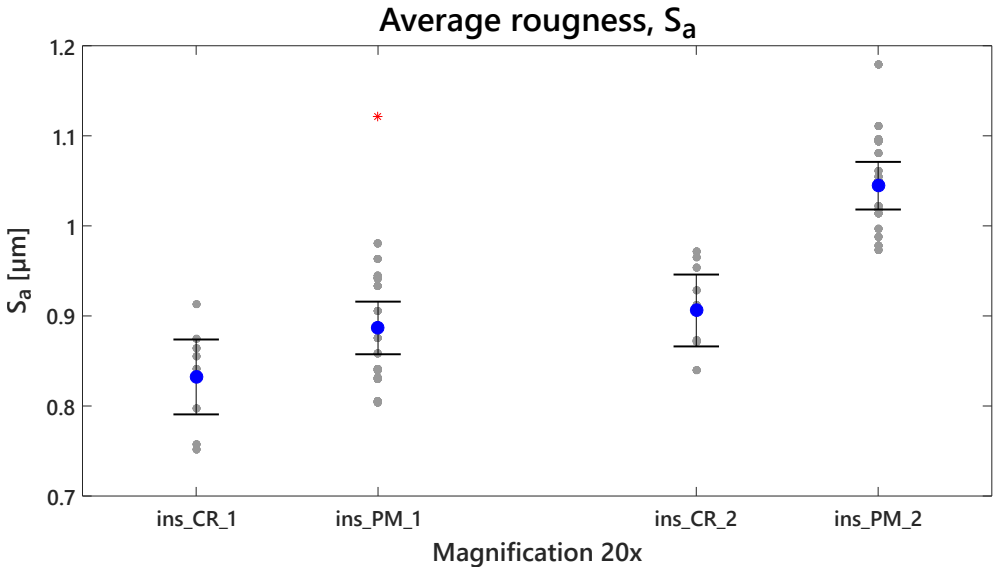

Figure A.2 – Average roughness $\mathbf{S_a}$ of the two CR and PM surfaces.

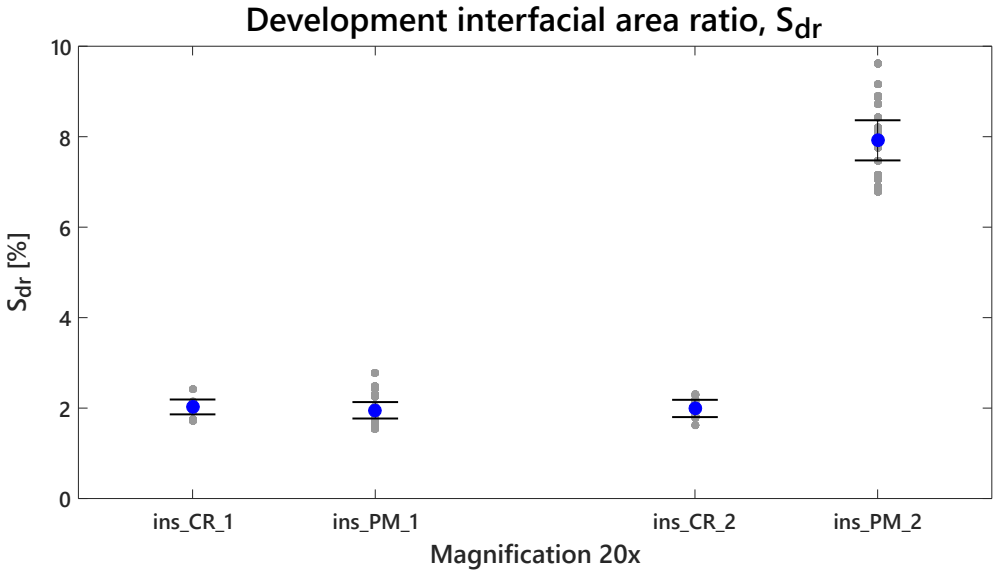

Figure A.3 – Development interfacial area ratio $\mathbf{S_{dr}}$ of the two CR and PM surfaces.

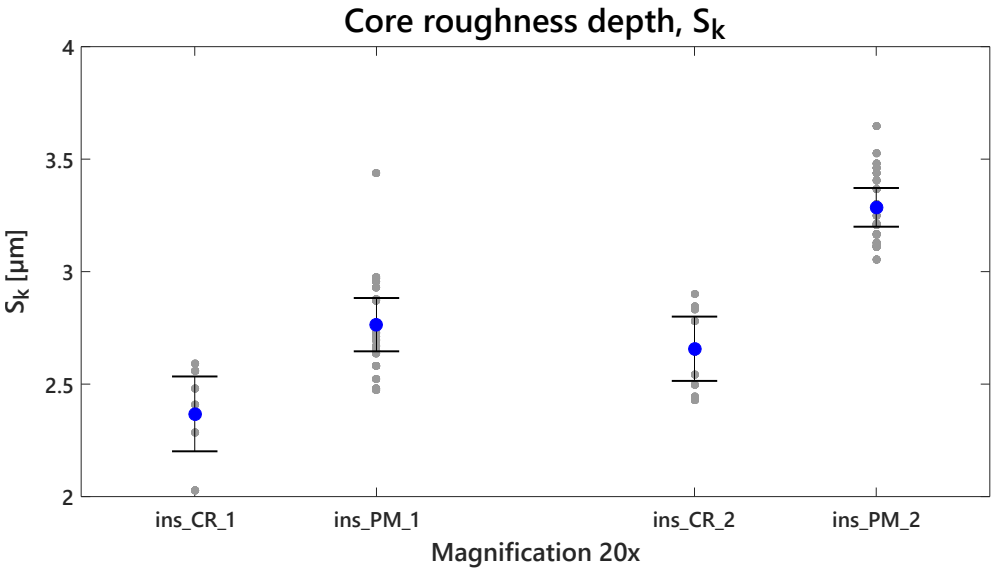

Figure A.4 – Core roughness depth $\mathbf{S_k}$ of the two CR and PM surfaces.

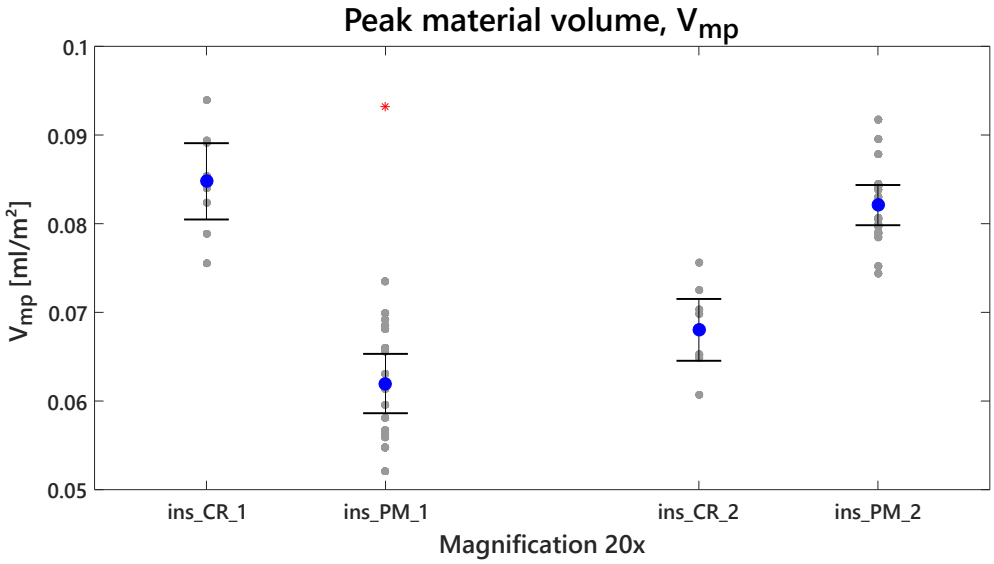

Figure A.5 – Peak material volume $\mathbf{V_{mp}}$ of the two CR and PM surfaces.

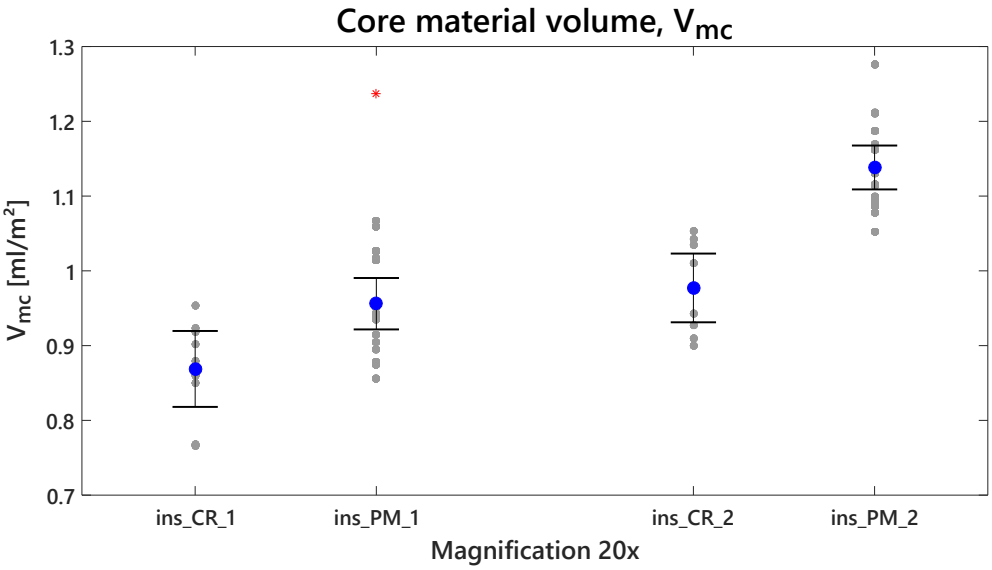

Figure A.6 – Core material volume $\mathbf{V_{mc}}$ of the two CR and PM surfaces.

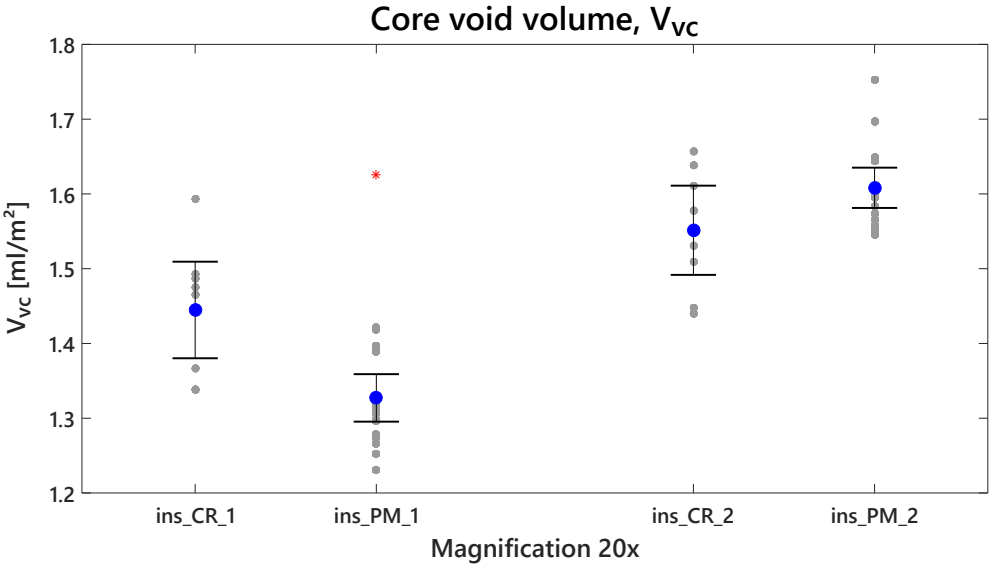

Figure A.7 – Core void volume $\mathbf{V_{vc}}$ of the two CR and PM surfaces.

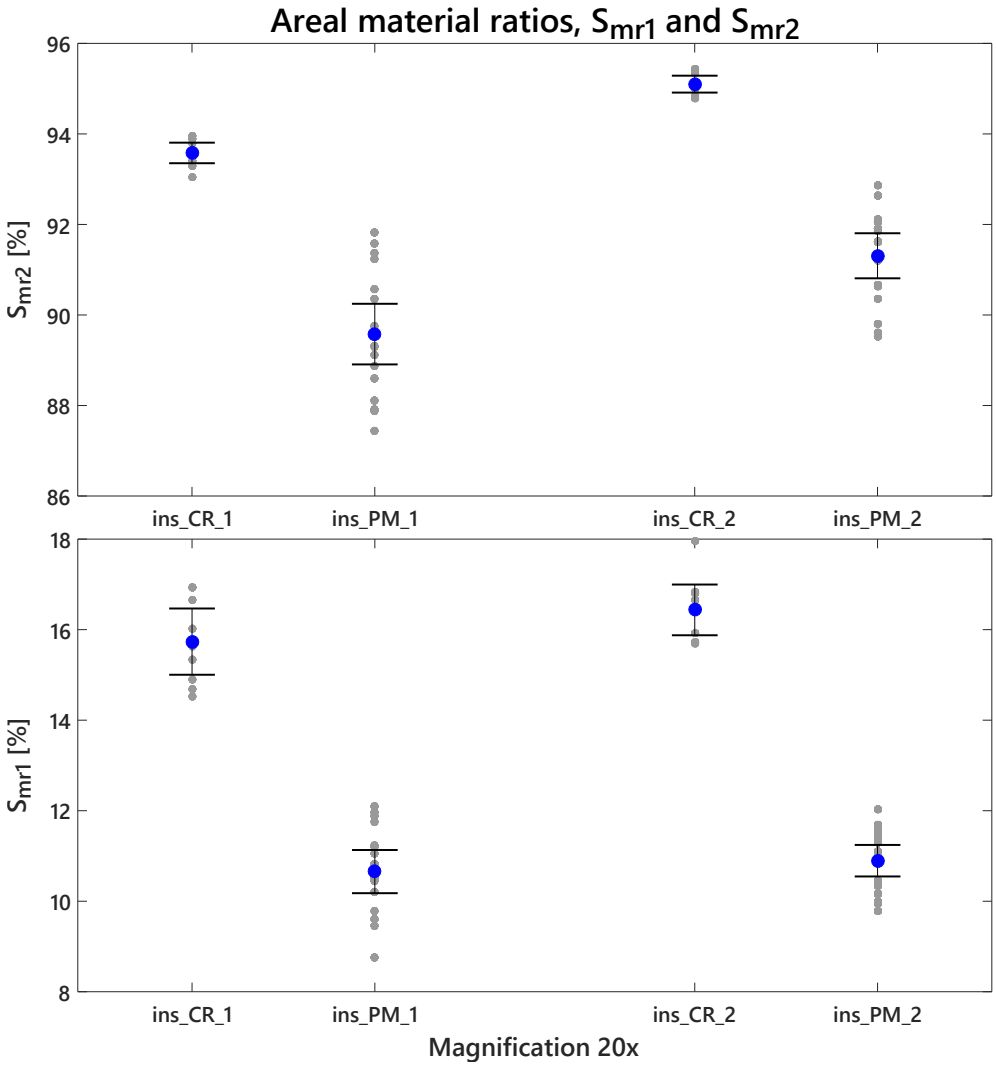

Figure A.8 – Areal material ratios $\mathbf{S_{mr1}}$ and $\mathbf{S_{mr2}}$ of the two CR and PM surfaces.

B Diagrams used in property evaluation

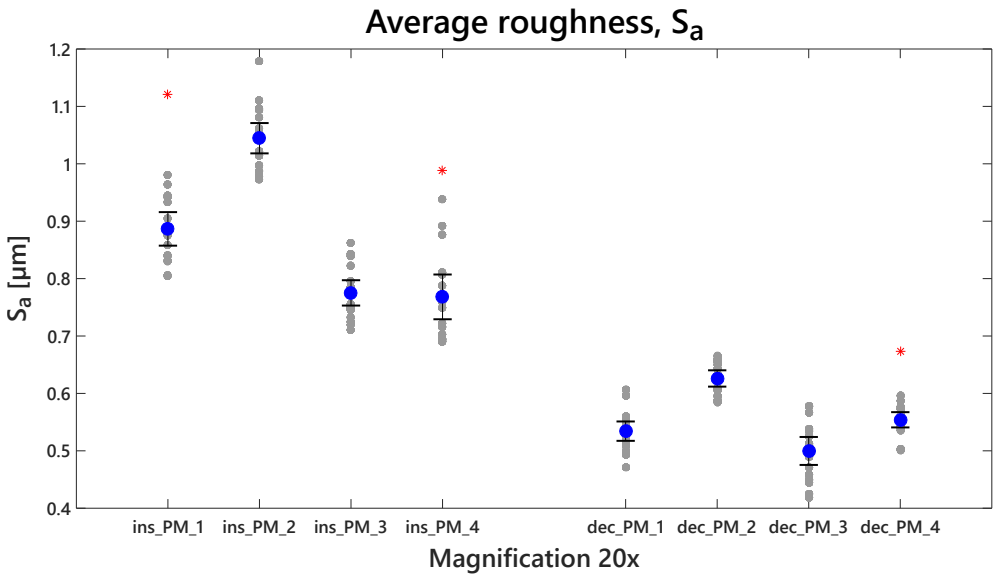

Figure B.1 – Average roughness $\mathbf{S_a}$ of all the inside and the décor PM sample surfaces.

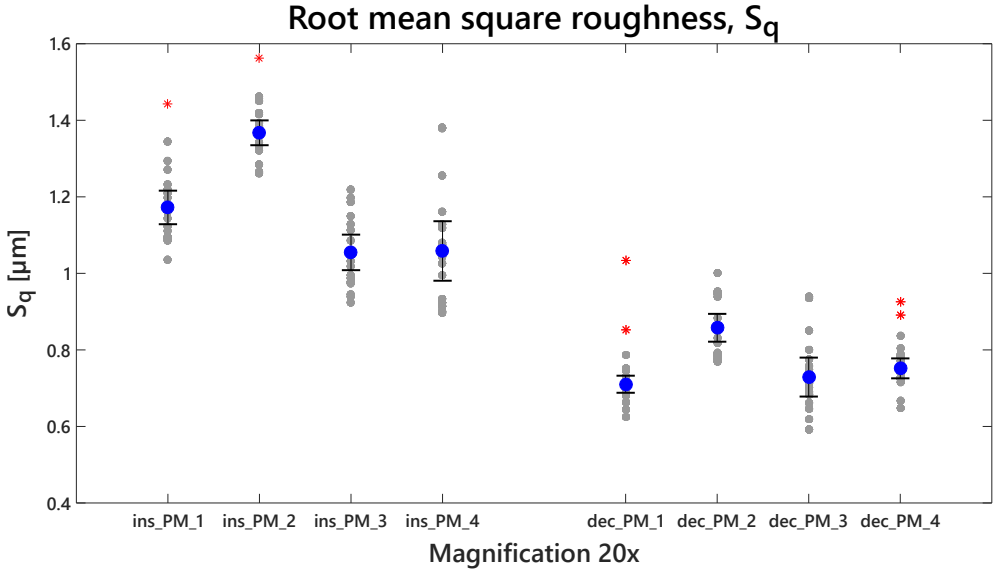

Figure B.2 – Root mean square roughness $\mathbf{S_q}$ of all the inside and the décor PM sample surfaces

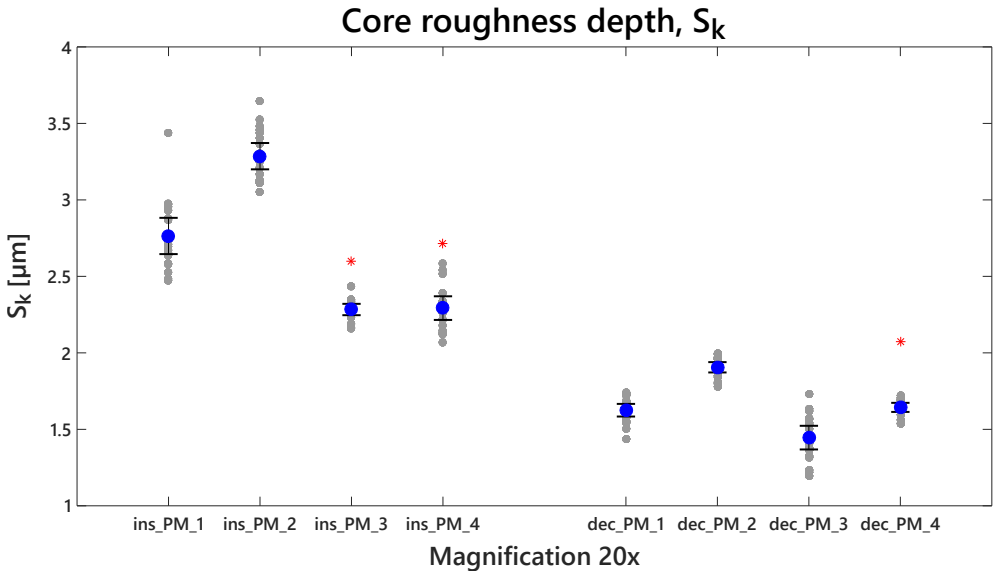

Figure B.3 – Core roughness depth $\mathbf{S_k}$ of all the inside and the décor PM sample surfaces

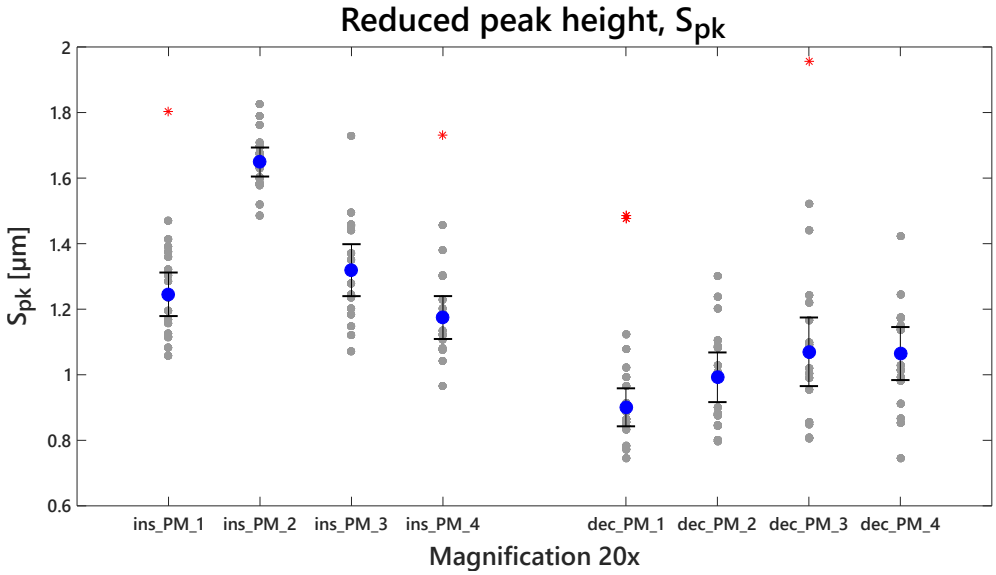

Figure B.4 – Reduced peak height $\mathbf{S_{pk}}$ of all the inside and the décor PM sample surfaces

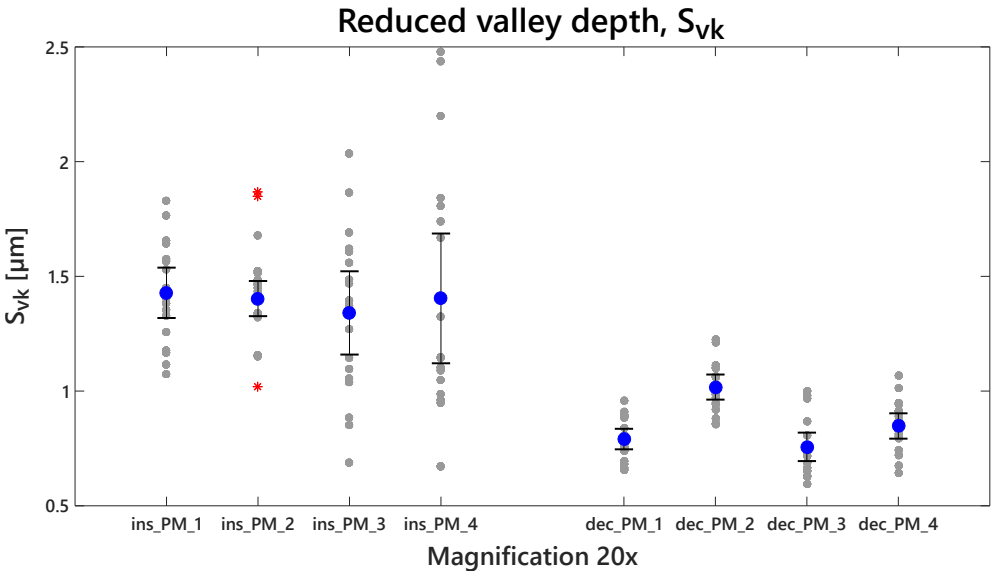

Figure B.5 – Reduced valley depth $\mathbf{S_{vk}}$ of all the inside and the décor PM sample surfaces

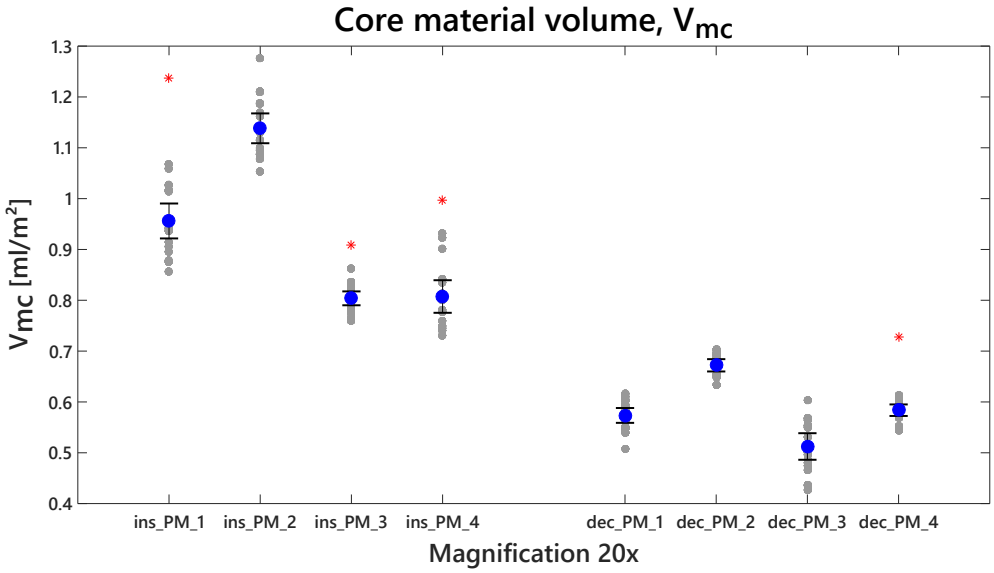

Figure B.6 – Core material volume $\mathbf{V_{mc}}$ of all the inside and the décor PM sample surfaces

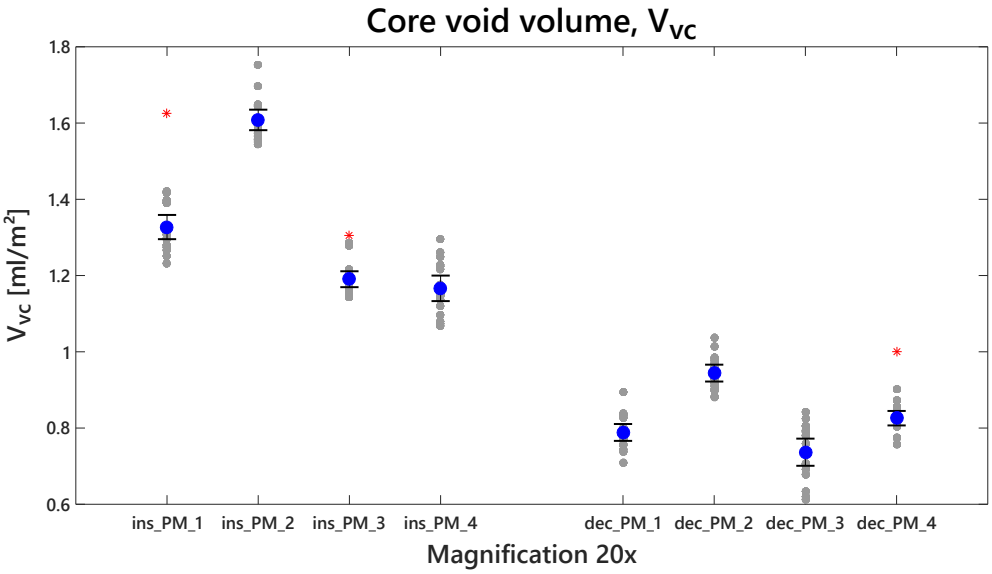

Figure B.7 – Core void volume $\mathbf{V_{vc}}$ of all the inside and the décor PM sample surfaces

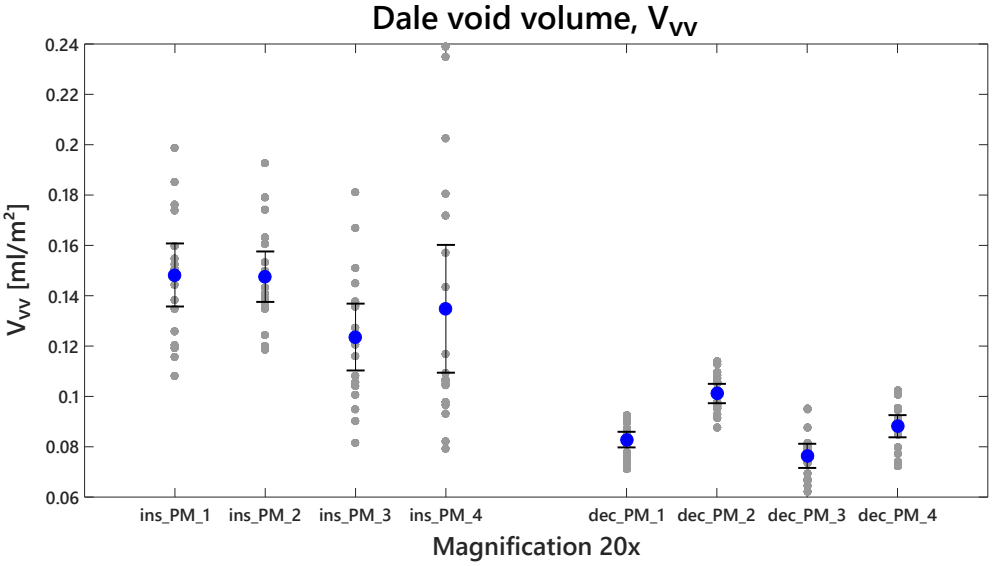

Figure B.8 – Dale void volume $\mathbf{V_{vv}}$ of all the inside and the décor PM sample surfaces